UPTEC E14001
Examensarbete 30 hp
Januari 2014

Cooling methods for electrical machines

Simulation based evaluation of cooling fins found on low voltage general purpose machines

Anders Karlsson

Påbyggnadsprogrammet till civilingenjörsexamen i elektroteknik
Master Programme in Electrical Engineering

UPPSALA
UNIVERSITET

Teknisk- naturvetenskaplig fakultet
UTH-enheten

Besöksadress:
Ångströmlaboratoriet
Lägerhyddsvägen 1
Hus 4, Plan 0

Postadress:
Box 536
751 21 Uppsala

Telefon:
018 – 471 30 03

Telefax:
018 – 471 30 00

Hemsida:
http://www.teknat.uu.se/student

Abstract

Cooling methods for electrical machines

Anders Karlsson

The main goal of this thesis project is to identify interesting concepts related to cooling of electrical motors and generators which could be evaluated using suitable computer simulation tools.
As the project proceeded it was decided to focus on investigating how the air from a fan flows along the finned frame of a general purpose low voltage electrical machine, how the heat is transferred between the frame and the cooling air and what the temperature distribution looks like. It was also investigated if it is possible to make improvements in the effectiveness of the cooling without adding additional coolers. This investigation focused on varying the fin design and evaluating the resulting temperature distribution. Due to the complex nature of the simulations a segment, and not the full frame, was considered.
Simulation model validation was performed through comparing air speed measurements that were performed on two different machines with the corresponding simulated air speed. The validation showed that good agreement between simulated and measured air speeds are obtained.
The conclusion from the simulations is that slight modifications to the current fin design could increase the cooling effect of the finned surface. The air velocity measurements also indicate that the cooling of the machines surface could potentially be improved by small changes in the exterior of the frame.

Handledare: Kristian Rönnberg
Ämnesgranskare: Juan de Santiago
Examinator: Nora Masszi
UPTEC E14001
Sponsor: ABB

Sammanfattning

Målet med detta examensarbete var att identifiera intressanta koncept relaterade till kylning av elektriska maskiner och generatorer, som kunde utvärderas med lämplig programvara för datorsimuleringar.

Under projektets gång så bestämdes det att fokusera på hur luften från en fläkt flödar längs med en generell lågspänningsmaskin, hur värmen överförs från ramen till den omgivande luften och hur temperaturfördelningen ser ut. Det undersöktes även om det var möjligt att förbättra effektiviteten av kylningen utan att ansluta extra kylanordningar. Undersökningarna fokuserades på olika fendesigner och dess påverkan på värmefördelningen. På grund av simuleringarnas komplexitet så har simuleringarna endast utförts på ett segment istället för hela maskinen.

Validering av simuleringarna utfördes genom att jämföra de simulerade lufthastigheterna med verklig lufthastighet som mättes på två maskiner i testmiljö. Valideringen visade att simuleringarna överensstämmer väl med de mätningar som utfördes.

Slutsatsen utifrån simuleringarna är att mindre förändringar av fenornas nuvarande design kan förbättra fenornas kylningsförmåga. Mätningarna av lufthastigheten ger även indikationer på att kylningen av maskinens utsida eventuellt kan förbättras genom små förändringar av ramens exteriör.

Foreword

I would like to thank my supervisor Kristian Rönnberg for all the help, feedback and discussions during the entire project. My thanks also go to Reza Moghaddam that helped me getting started and choosing what this thesis would focus on. Also thanks to Annelie Lönnholm who helped me with all the administrations. All the people at ABB, both staff and thesis workers have made me feel really welcomed at ABB.

Last but not least I would like to express my deepest gratitude to my family for being supportive and encouraging during this time, especially my girlfriend Frida Johansson.

TABLE OF CONTENTS

1 INTRODUCTION

1.1 Purpose

An electrical machine generates heat in its various parts because of mechanical losses, magnetic losses and electrical losses. To reduce the electrical losses and thereby the heat in the copper windings, the area of the windings are increased. Copper is however an expensive and limited natural resource. If the machine can be cooled more efficiently, the amount of copper that is used can be decreased and therefore make the machine more cost effective and reduce the amount of material needed for the machine.

The purpose of this report is to present the findings from my master thesis project focused on electrical machine cooling

The initial part focused on literature study in order to gather sufficient understanding of the theory behind heat transfer and how this theory can be applied to electrical machines. After a thorough review of the information gathered, it was decided to investigate the performance of the cooling fins commonly found on fan cooled electrical machine, and if the cooling could be improved just by changing the design of the fins. The investigation was pursued by computer simulations of the airflow and heat distribution where different designs were compared. Airflow measurements were also performed on an actual machine in order to gather data to be used for validation purposes, and in order to determine suitable input data for the numerical models.

1.2 Definitions

CHT	Conjugate heat transfer
SPF	Single phase flow
HT	Heat transfer in solids
NITF	Non isothermal flow
DE	Drive end
NDE	Non drive end

1.3 Structure

This report has the following structure.

Section 1 Introduction (this section) describes the purpose for this report as well as definitions and structure.

Section 2 Problem Description describes what the problems are with external forced cooling of an electrical machine

Section 3 Theory describes what will have an impact on the airflow and the different kinds of heat transfer. Also the theory of different fin designs and software is described.

Section 4 Measurements explain how the air velocity measurements have been done and the results of them

Section 5 Simulations explains all the settings for the different models and the results of them

Section 6 Results compare the results from the measurements and the simulations

Section 7 Discussion, here the results, future work, problems and sources of errors are discussed.

2 DESCRIPTION OF THE PROBLEM

Today electrical machines are commonly used in the industry. It is desirable to have machines which are as small, efficient and long lasting as possible, requiring as little maintenance as possible. To be able to make the machines smaller without reducing the power, or to get more power without increasing the size of the machine, it is important to get a better cooling of the machine, preferably without adding external coolers. A common way to cool the machine is to have a fan mounted at the NDE of the machine which pushes air along fins, which are commonly found to run along the axial direction of the machine. This will give a good cooling in the NDE but the cooling is decreased along the machine. Since it is the warmest part of the machine that sets the limit, it is desirable to have a more efficient and even distribution of the cooling.

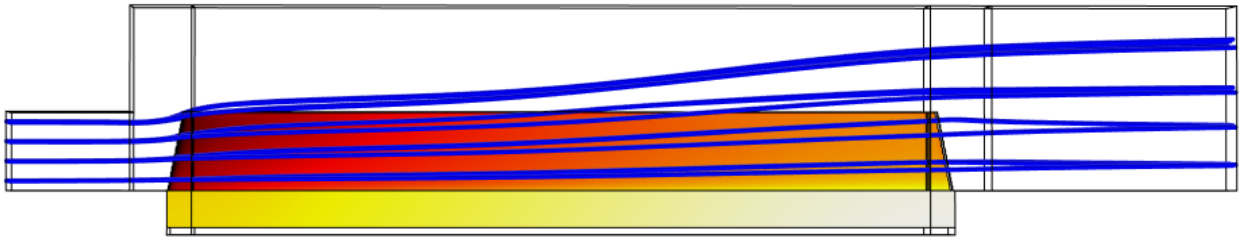

Figure 1: The red color of the fins and stator illustrates the cool area and the yellow/white parts are warmer area. The blue lines shows the path of the airflow

2.1 Deviating airflow

On a machine with a fan mounted on the NDE, air will flow along the sides of the machine to cool the external fins whose purpose is to lead away heat from the interior of the machine.

Air that flows along a surface will experience a reduction in velocity due to surface friction. The friction force will cause a slow moving boundary layer. This boundary layer will “push” the moving air away from the surface. Due to the fin design, that forms ducts in which air is supposed to flow, there will be a large surface area on which this boundary layer can form. This will force the air out of the ducts, causing a reduction of the cooling effect on the machine as compared to if the air was flowing in the duct all the way from inlet to outlet. The deviating airflow can be seen as blue lines in Figure 1.

2.2 Temperature distribution

A fan is mounted on the NDE of the machine, pressing air along the sides of the machine. As the air will flow along the sides of the machine the air will get warmer from the heat of the machine. Because of this the machine will be efficiently cooled close to the fan but the further the distance is from the fan the less efficiently the air will cool the machine, causing an uneven temperature distribution on the machine. This uneven temperature distribution can be seen as red and yellow colours in Figure 1.

2.3 Fin design

Laminar flow of the air does not transport away the heat from the fins as efficiently as turbulent flow [1]. Is it possible to get a more efficient cooling by changing the design of the fins to create more turbulence?

3 THEORY

3.1 Airflow

Airflow investigations, through measurements and numerical modelling, became the major task during the execution of this thesis project. A significant portion of time, due to the complexity involved in airflow modelling, was spent on developing the numerical models used for describing the airflow. An introduction to each phenomenon considered during the modelling effort is given below.

Density variation due to air speed

Density variations due to the air speed will not become apparent until the air reaches speeds around one third of the speed of sound[1]. As a consequence density variations due to the flow speed are commonly neglected in low air speed situations [2]. Therefore air will be considered incompressible in the rest of this report, since the air speeds encountered are well below 100 m/s.

Surface friction

Close to walls frictional effects have to be considered. The friction on the fluid, caused by the presence of a wall, will cause a boundary layer to form. This boundary layer will increase in size along a long surface. In Figure 2a one can see how the velocity is equally large over the entire cross section at an inlet. In Figure 2b the velocity is starting to decrease close to the wall due to wall friction. In figure c a fully developed friction flow has formed and the velocity vectors display a parabolic shape.

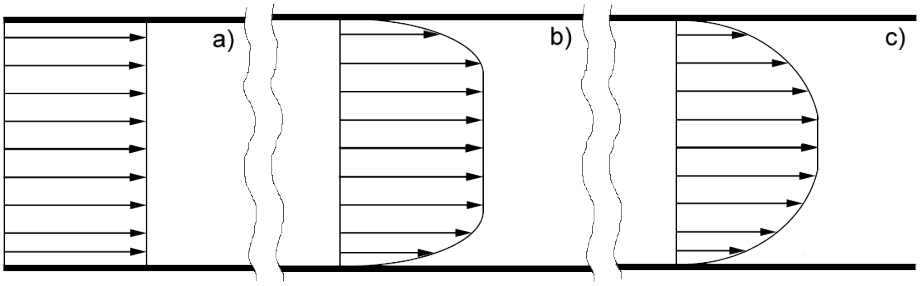

Figure 2a-c: Figure 1a shows the air velocity at the inlet. Figure 1b shows how the velocity decreases along the walls. Figure 1c shows a fully developed frictional flow that will finally occur.

Laminar and turbulent airflow

There are two different kinds of flow, laminar and turbulent. Laminar flow displays a smooth and parallel flow. It the length of the airflow is sufficiently long or if the airspeed increases, the airflow character will change to an irregular and finally to a chaotic pattern, which is referred to as turbulent flow [3]. There are big differences in heat transfer and forces between laminar and turbulent flow. Laminar flow is relatively easy to calculate since it always has the same velocity, density and pressure, independent of time and is therefore called a stationary flow. When the airflow is used for cooling it is preferable to have turbulent flow

[1] Speed of sound is 340 m/s in room temperature air

since it is much more efficient in transporting the heat. As can be seen in Figure 3 the velocity gradient is larger close to the walls when the air is turbulent compared to when laminar. However turbulent flow is rather difficult to calculate since the flow and pressure will change constantly. Therefore turbulent flow is time dependent. Despite that, it is sometimes possible to calculate turbulent flow as stationary with an average value [2]. When air flows between constraining walls the viscous forces are more prominent near the walls than in the center line [1]. When the air velocity increases the inertia forces will increase until they overcome the viscous force in the center. A turbulent flow with vortices will then start to form in the centerline while there still is laminar flow close to the walls. If the air velocity increases further, the turbulent flow in the center will spread from the center until the entire flow is turbulent as shown in Figure 3. When the laminar flow that has a parabolic velocity gradient curve turns to turbulent flow the gradient curve will also start to flatten out. Because of this the turbulent flow is more efficient to transport heat away from the surrounding walls

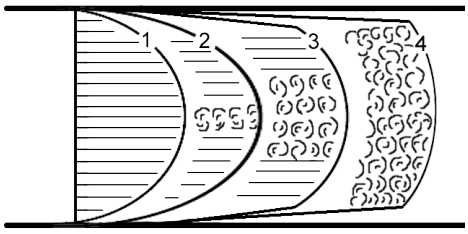

Figure 3: 1=Viscous flow, Re<1200. 2=Critical velocity, Re~1200. 3=Turbulent flow, Re>1200. 4=Full turbulent flow, Re~4200

Reynolds number

Reynolds number is a dimensionless number that gives the ratio of inertial forces to viscous forces and is used to characterize different flow regimes. At low Reynolds number (<1200) where viscous forces are dominant the flow will mainly exhibit laminar characteristics. At high Reynolds number (>4000) where inertial forces are dominant there will be vortices and other flow instabilities mainly corresponding to the turbulent flow regime. The Reynolds number between 1200 and 4000 is called the critical number and is the region where laminar flow is turning to turbulent and they can both exist as in Figure 3. These numbers are not exact but are more used as a hint on what airflow is expected. Things that also may have influence on the type of flow addition to the Reynolds number are geometry, surface roughness, temperature, other disturbances of flow as inlet etc. The Reynolds number for internal flow in circular pipe can be calculated with equation (1)

$$Re = \frac{U \cdot L}{v} = \frac{\rho \cdot U \cdot L}{\mu} = \frac{Inertial\ force}{Viscous\ force} \qquad (1)$$

where ρ is the fluid density [kg/m^3], μ is fluid viscosity [Pa*s or N*s/m^2 or kg/m*s], v=μ/ρ is the kinematic viscosity [m^2/s], and U and L are velocity [m/s] and length [m] (diameter in this case) that characterize the scale of the flow. For noncircular pipes the length L in equation (1) is replaced by the hydraulic diameter D_h. The formula for D_h can be found in equation (2)-(5).

Circular tube:

$$D_h = \frac{4(\pi \cdot D^2/4)}{\pi \cdot D} = D \tag{2}$$

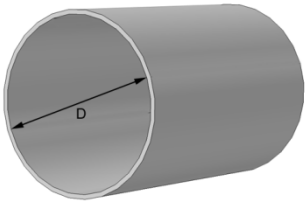

Square duct:

$$D_h = \frac{4a^2}{4a} = a \tag{3}$$

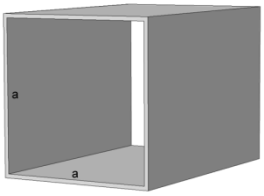

Rectangular duct:

$$D_h = \frac{4 \cdot a \cdot b}{2(a+b)} = \frac{2 \cdot a \cdot b}{a+b} \tag{4}$$

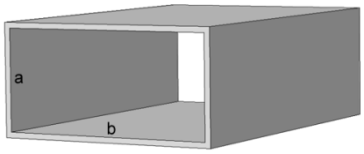

Channel:

$$D_h = \frac{4 \cdot a \cdot b}{2 \cdot a + b} \tag{5}$$

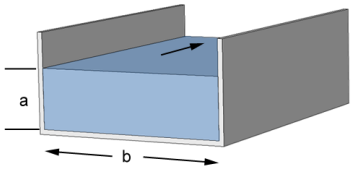

When there is a free surface as in open channel flow the wetted perimeter includes only the walls in contact with the fluid so the surface that is in contact with air is not included [3].

3.2 Heat

Even though cooling/heat of electrical machines is the main goal of this thesis it is easier and less time consuming to calculate heat compared to the airflow. As can be seen in Figure 4, there are three different kinds of heat transfers: radiation, conduction and convection.

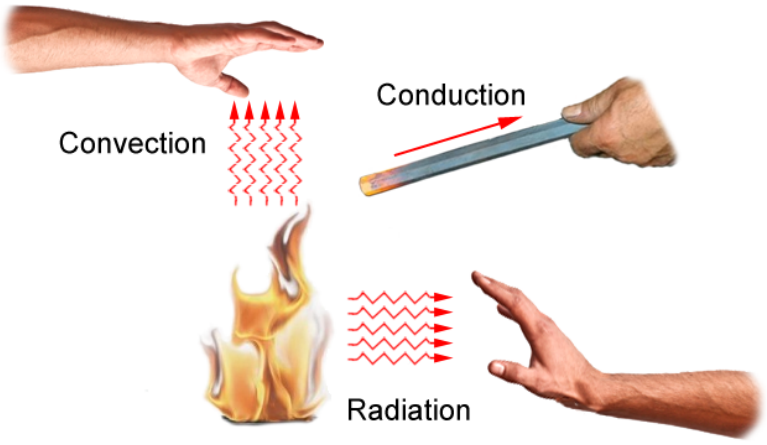

Figure 4: Illustrates the different kinds of heat transfer

Radiation

Radiation is the energy emitted by matter in the form of electromagnetic waves or photons. Heat transfer by radiation is the fastest heat transfer and it suffers no damping in vacuum. Thermal radiation is emitted by all material (above absolute zero) because of its temperature. It should not be confused with other radiation like gamma rays and x-rays that are not related to temperature. The rate of radiation that can be emitted from a surface is given by the Stefan-Boltzmann law [3] and is given in equation (6)

$$Q_{emit} = \varepsilon \cdot \sigma \cdot A_s \cdot T_s^4 \ [W] \tag{6}$$

where ε is the emissivity of the surface. Its value is in the range of $0 \leq \varepsilon \leq 1$ and is a measure of how closely a surface is to a "black body" which is the idealized surface that emits radiation at the maximum rate. $\sigma = 5{,}670 \cdot 10^{-8}\, W/m^2 \cdot K^4$ is the Stefan-Boltzman constant, A_s is the surface area through which heat radiation take place and T_s is the surface temperature. Another important parameter is a surface absorptivity α which is in the range of $0 \leq \alpha \leq 1$. It is the fraction of how much energy is absorbed by the surface where a black body has the value of α=1

Conduction

Conduction is the transfer of heat or energy from more energetic particles to less energetic ones. The transfer can take place in solids, liquids or gases. The rate of heat conduction depends on the material, geometry, thickness and the temperature differences. The thermal conductivity of a material tells how good the heat transfer is in that material. The higher thermal conductivity a material has the better conductor it is and the lower thermal conductivity the greater insulator it is. Examples of materials with different conductivities can be seen in Table 1.

Table 1: Examples of thermal conductivity on different materials[4]

Material	Thermal conductivity [W/(mK]
Silver	418
Copper	400
Iron	82
Water	0,6
Air	0,026

Convection

Convection is the energy transfer from a solid surface to an adjacent moving liquid or gas. If the gas or liquid is not moving then it is not convection but pure conduction. The faster the fluid motion is the greater the convective heat transfer is. Convection is called forced convection if the fluid is forced to move by an external force like a fan or the wind. It is called natural convection when the movement of the fluid is due to natural means such as the buoyancy effect, which manifests itself as the rise of warmer and thus lighter fluid and the fall of cooler and thus denser fluid. The rate of heat convection is expressed in equation (7) by Newton's law of cooling [3]:

$$Q_{conv} = h \cdot A_s(T_s - T_\infty)\ [W] \qquad (7)$$

Where h is the convection heat transfer coefficient in W/m2*K, A_s is the surface area through which convection heat transfer take place, T_s is the surface temperature and T_∞ is the temperature of the fluid on a distance far away. On the surface the fluid and the material will have the same temperature. The convection heat transfer coefficient h is not a property of the fluid but experimentally determined by all the variables influencing convection such as the properties of the fluid, surface geometry, bulk fluid velocity and the nature of fluid motion.

3.3 Fin equations

Even though an analytical treatment of heat transfer over a finned surface study is not included in the scope of this report, the analytical theory introduces useful concepts which will be referred to later in this report. Therefore, the basic concepts in the analytical treatment of finned surfaces are introduced here. A deeper presentation of this topic is given in [3]

When having a piece of volume from a fin at location x with length Δx, cross sectional area of A_c and a perimeter of p, when neglecting radiation the energy balance on this volume can under steady conditions be expressed as:

$$\dot{Q}_{cond,x} = \dot{Q}_{cond,x+\Delta x} + \dot{Q}_{conv}$$

Where $\dot{Q}_{cond,x}$is the rate of heat conduction into the element at x, $\dot{Q}_{cond,x+\Delta x}$ is the rate of heat conduction from the element at $x+\Delta x$ and $\dot{Q}_{conv}$ is the rate of heat convection from the element [3]. When setting $A_s=p\Delta x$ *in* equation (7) we get

$$\dot{Q}_{conv} = h \cdot (p\Delta x)(T_s - T_\infty)\ [W] \qquad (8)$$

Substituting and dividing by Δx, we obtain

$$\frac{\dot{Q}_{cond,x+\Delta x} - \dot{Q}_{cond,x}}{\Delta x} + hp(T - T_\infty) = 0 \quad (9)$$

Taking the limit as $\Delta x \to 0$ gives

$$\frac{d\dot{Q}_{cond}}{dx} + hp(T - T_\infty) = 0 \quad (10)$$

From fourier's law of heat conduction we have

$$\dot{Q}_{cond} = -kA_c \frac{dT}{dx} \quad (11)$$

Substitution of this relation into equation (10) gives the differential equation governing heat transfer in fins

$$\frac{d}{dx}\left(kA_c \frac{dT}{dx}\right) - hp(T - T_\infty) = 0 \quad (12)$$

In general, when x changes so does the cross section area A_c, and the perimeter p. This makes the differential equation (12) difficult to solve.

Convection from fin tip

Solving the general equation for convection from a fin tip is a rather complex task. Instead an approximation can be used that is yet practical and accurate. To calculate the loss of the tip one can replace the fin length L by a corrected fin legth L_c defined as

$$L_c = L + \frac{A_c}{p} \quad (13)$$

Where A_c is the cross-sectional area and p is the perimeter of the fin at the tip. Multiplying this with the perimeter gives $A_{corrected}=A_{fin\ (lateral)} + A_{tip}$ which indicates that the fin area determined using the corrected length is equivalent to the sum of the lateral fin plus the fin tip area. Therefore fins with convective tips can be treated as fins with insulated tips as in Figure 5a-b by replacing the actual fin length by the corrected length for adiabatic fin tip in formula for heat distribution

$$\frac{T(x) - T_\infty}{T_b - T_\infty} = \frac{\cosh m\,(L - x)}{\cosh mL} \quad (14)$$

and the rate of heat transfer

$$\dot{Q}_{adiabatic\ tip} = -kA_c \frac{dT}{dx}\Big|_{x=0} = \sqrt{hpkA_c}(T_b - T_\infty)\tanh mL \quad (15)$$

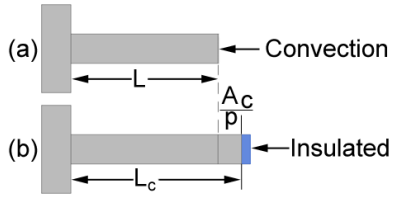

Figure 5a-b: Heat transfer from the corrected fin length with insulated fin tip in figure 3b is equal to heat transfer from actual length of fin with convection from fin tip in figure 3a

Fin efficiency

Heat is transferred from a surface to the surrounding medium by convection with the heat transfer coefficient of h. When disregarding radiation or accounting for its contribution in the convection coefficient h, heat transfer from a surface area A_s is expressed by $\dot{Q} = hA_s(T_s - T_\infty)$. If we then have a fin with constant cross-sectional area that is attached with perfect contact on a surface heat will be transferred by conduction from the surface to the fin and then by convection from the fin to the surrounding medium. For simplicity the fin tip can be a assumed to be adiabatic by using the corrected length for the fin instead of the actual length. The maximum heat transfer from the fin is the maximum at the bottom of the fin

$$\dot{Q}_{fin,\ max} = hA_{fin}(T_b - T_\infty) \tag{16}$$

but in reality the temperature drops along the fin and therefore the heat transfer from the fin is less because of the decreasing temperature difference $T(x) - T_\infty$ toward the fin tip. To account for this temperature decrease in the heat transfer, a fin efficiency is defined as

$$\eta_{fin} = \frac{\dot{Q}_{fin}}{Q_{fin,\ max}} = \frac{Actual\ heat\ transfer\ rate\ from\ the\ fin}{Ideal\ heat\ transfer\ rate\ from\ the\ fin\ if\ the\ entire\ fin\ were\ at\ base\ temperature} \tag{17}$$

Since fins with triangular or barabolic shape is made of less material and more efficient then fins with rectangular shape they are more suitable when less weight and low price is desirable. The efficiency for different shapes can be seen in appendix 1

Fin effectiveness

The overall effectiveness for a finned surface can be calculated with equation (18) which gives a ratio of the total heat transfer from a finned surface compared to the heat transfer from the same surface without fins.

$$\varepsilon_{fin,overall=} \frac{\dot{Q}_{total,\ fin}}{\dot{Q}_{total,\ no\ fin}} = \frac{h(A_{unfin} + \eta_{fin}A_{fin})(T_b - T_\infty)}{hA_{no\ fin}(T_b - T_\infty)} = \frac{A_{unfin} + \eta_{fin}A_{fin}}{A_{no\ fin}} \tag{18}$$

An effectiveness of ε_{fin}=1 means that the fins have no contribution on the heat transfer. If ε_{fin}<1 then the fins acts as an insulation that impedes the heat transfer. When ε_{fin}>1 the heat transfer is enhanced but ε_{fin} has to be sufficiently larger than 1 to be justified due to the extra cost for the material and weight. Both the effectiveness and the efficiency are related to the performance of the fins but they are different quantities. However since they are related to each other one of them can easily be determined if the other one is known as can be seen in equation (19)

$$\varepsilon_{fin}=\frac{\dot{Q}_{fin}}{\dot{Q}_{no\ fin}}=\frac{\dot{Q}_{fin}}{hA_b(T_b-T_\infty)}=\frac{\eta_{fin}hA_{fin}(T_b-T_\infty)}{hA_b(T_b-T_\infty)}=\\ =\frac{A_{fin}}{A_b}\eta_{fin} \tag{19}$$

Length of a fin

One basic rule is that the more surface the more heat transfer there will be. However since the temperature drops exponentially along the fin until the temperature is the same as the environment there is a limit on how long the fin can be to contribute to the heat transfer. If the fin gets to long the extra length will only contribute to excessive weight, increased size, material waste, extra cost and it will suppress the fluid motion. To be able to determine a proper length of the fin we can compare the heat transfer from a fin with finite length and one with infinite length under the same conditions. The heat transfer ratio will be

$$\frac{\dot{Q}_{fin}}{\dot{Q}_{long\ fin}}=\frac{\sqrt{hpkA_c}(T_b-T_\infty)\tanh mL}{\sqrt{hpkA_c}(T_b-T_\infty)}=\tanh mL \tag{20}$$

When mL= 5 the fin can be considered to be infinitely long. If mL is reduced to half (mL=2.5) the heat transfer will be only drop 1 percent as can be seen in Table 2. To get a good compromise between heat transfer and fin size one can set mL=1 which will correspond to a 76,2 percent increase in heat transfer.

Table 2: Variation of heat transfer with different length of the fin

mL	$\frac{\dot{Q}_{fin}}{\dot{Q}_{long\ fin}}=\tanh mL$
0,1	0,100
0,2	0,197
0,5	0,462
1,0	0,762
1,5	0,905
2,0	0,964
2,5	0,984
3,0	0,995
4,0	0,999
5,0	1,000

4 NOTES ON THE UTILIZED SIMULATION TOOL

4.1 COMSOL Multiphysics

The software that is used to solve problems in this master thesis is COMSOL multiphysics 4.3b. There are big differences in some areas in this software depending on what version is used so a model that is designed in one version of Comsol might not work in a different version without doing some changes. COMSOL multiphysics is a software that use FEM[2] when solving models. The software makes it possible to solve both the airflow distribution and its contribution of cooling. It contains several kinds of physic modules that can be added to the project depending on what one want to solve.

4.2 Geometry

There are basicly three ways to get the desired geometry in COMSOL [5]. The first one is to design the geometry in some CAD-software, export it and then import it into COMSOL. COMSOL CAD import supports most of the major software. This way the geometry is locked and the dimensions cannot be changed within COMSOL. The second way is to use livelink[3] that for geometry purpose supports Pro/ENGINEER and SolidWorks. Then the COMSOL and the CAD software are synchronized so geometry and parameters can be changed in either of the softwares. The third way is to design the geometry directly in COMSOL. For simpler geometry this is an easy way and it is very convenient when using variable parameters for the design but it does not take much, especially in 3D to find the limits of the built in CAD design. The standard setting for COMSOL is to use a CAD import module kernel for geometry representation even if the design is made entirely within COMSOL. However this require the use of the cad import license so if possible one should change the geometry representation setting to use COMSOLs kernel instead and thereby not occupy the CAD import license if not necessary. This can also be done under settings in COMSOL so this will be set for all future models.

4.3 Mesh

When solving a problem in COMSOL the model has to be broken down into smaller pieces. This is called meshing and is one of the major problems when calculating fluids. The mesh may consist of tetrahedral, hexahedral, prism, or pyramid mesh elements. It is sometimes possible to do a simulation with a very coarse resolution but the result might not be correct even though no warning is displayed. To be certain the results are accurate in the simulation one has to run simulations with a finer and finer mesh until the different results does not differ more than what is acceptable. The finer mesh that is used the more domain elements is created and therefore it takes longer to run a simulation. This is a balance that can be difficult to determine for the inexperienced. There are different ways to reduce the amount of meshing but still get an accurate result.

[2] Finite element method is a numerical method for finding approximate solutions to differential equations together with a set of additional restraints

[3] Requires a special license

First and foremost one should investigate if there is symmetry in the model. Preferably one should do the model in 2D since it will reduce the mesh and solution time considerably. If that is not possible it might be possible to reduce the model to a slice of the original model that will still show the same results. For example in this project only two cooling fins are used since they will show the same results as if ten fins would be used. As default meshes will be finer near edges and especially sharp edges. Therefore it is good to avoid sharp edges in the design when possible, or at least in air domains. Once the design of the geometry is decided it is time to design an efficient meshing. There are so many ways a mesh can be designed that this report will only consider how the design was made in this model. In geometries that are linear like smooth fins it is preferable if one can sweep the mesh. The reason for this is that it can reduce the amount of mesh elements and the mesh will look the same all the way along the fins. Otherwise there can be deviation in the results that depends on the mesh. Often a coarser mesh is used in the solid domains compared to the air domains since only heat will travel in the solids and that do not require as fine mesh as air do. When sweeping a mesh, quads are created along the mesh as can be seen in Figure 6. These quads cannot match with the tetrahedral that is created in the surrounding domains. If quad mesh will be abutting triangular mesh one has to convert the surface of the quads by inserting diagonal edges in the quads like in Figure 6

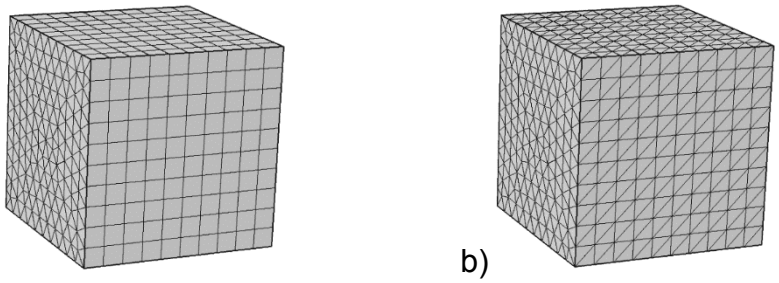

Figure 6a-b: In figure *a* quads are caused by swept mesh. In figure *b* diagonal edges are inserted

Airflow is also sensitive to surface resistance and therefore a finer mesh is required closest to the fins. There a meshing technique called boundary layer is used.

4.4 Physics

To solve something, Physics module has to be added. There are several physics module available but this report will only mention those relevant for this work. The ones that were used were: Turbulent flow k-ε, Heat transfer in solids and conjugate heat transfer.

Turbulent flow K-ε (K-epsilon)

Turbulent flow K-ε is one of the most used turbulence model for industrial applications. It contains of two transport equations and two dependent variables: the turbulent kinetic energy k, and the dissipation rate of turbulence energy ε. Even though the model is so common, it has some limitations[5]. The *k*-ε turbulence model is based on several assumptions, as that the Reynolds number

is high enough so there will be turbulent flow. Since these assumptions are not always true, the accuracy is limited. For example it does not respond correctly to flows with decreasing pressure gradients which can result in under-predicting the extension of recirculation zones. Also when the model describes rotating flows, it often shows poor agreement with experimental data. In most cases, this limited accuracy is a reasonable trade-off for the amount of computational resources saved compared to more complicated turbulence models. The airflow close to a solid wall is very different for turbulent flow compared to free stream. Because of this the assumptions used to derive the *k*-ε model are not valid close to walls. Even though it is possible to modify the *k*-ε model so that it will work for flow in wall regions it is not always desirable because it requires a very high resolution. To be able to describe the flow at the walls, an analytical expression that is known as wall functions is used instead. These functions are such that the computational domain is assumed to start at the distance δ_w from the wall as seen in Figure 7

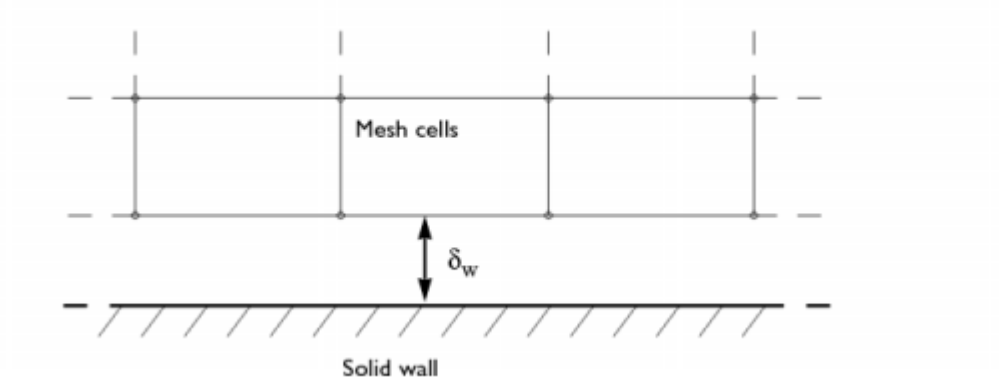

.

Figure 7: Shows the distance from the wall where the computational domain starts[5].

The distance δ_w is automatically computed so that

$$\delta_w^+ = \rho u_\tau \delta_w / \mu \tag{21}$$

where $u_\tau = C_\mu^{1/4}\sqrt{k}$ is the friction velocity, which becomes 11.06. This corresponds to the distance from the wall where the logarithmic layer meets the viscous. δ_w is limited from below so that it never becomes smaller than half of the height of the boundary mesh cell. This means that δ_w^+ can become higher than 11.06 if the mesh is relatively coarse. Therefore it is important to always investigate the solution to make sure that δ_w^+ is 11.06 on most of the walls. If δ_w^+ gets much higher than 11.06 over significant parts of the wall the results might not get as accurate as it is supposed to be.

Heat transfer in solids (HT)

In a machine heat is produced from eddy currents, resistive losses etc but this heat should be transported away by the fins. To simulate the cooling effect from the airflow on the fins heat has to be generated from the bottom of the model, simulating the heat from the rotor and stator inside the machine (from now on just called stator). It is possible to set a constant temperature on the stator but that would not give an accurate result since it would have the same temperature no matter how efficient the cooling would be. For simplicity silica glass is used in the model as a stator which is fed with an electrical power that generates heat in the material. This will have similar properties in the simulations as if a real stator with electrical windings would be used. When coupling fluid flow and heat transfer it is important to change in heat transfer in solids: heat transfer in fluid/model input/velocity field till velocity field(spf/fp1). The heat transfer in solids function uses

$$\rho C_p \frac{\partial T}{\partial t} - \nabla \cdot (k \nabla T) = Q \qquad (22)$$

Where ρ is the density, C_p is the heat capacity, k is the thermal conductivity and Q is a heat source or sink. Since *Q* is dependent of the volume of the stator it is important to remember that the heat dissipated in the stator changes with the volume of stator. This has to be taken under consideration if comparing models of different sizes. When two solids are pressed together one has to know the contact pressure and the microhardness of the softer material. The contact between two material can vary a lot, especially in electrical machines between the stator and frame due to the uneven surface of the stator caused by the stacked layer of metal sheets, as seen in Figure 8. This value can even vary on two identical machines[6].

Figure 8: Shows in a microscopic level how the contact can be made in several points between the stator and frame[5].

Non-isothermal flow (NITF) and Conjugate heat transfer (CHT)

NITF is almost equal to CHT. The difference between them is if it is the fluid or the solid that is used as the standard interface. NITF and CHT is a combination of turbulent SPF and HT. When using NITF or CHT one does not have to couple the fluent and heat transfer manually but instead this is solved automatically. When solving NITF or CHT (for turbulent flow only) an additional calculation is added for the turbulent heat flow and heat transfer in the solver compared to when just using SPF and HT. If one wants to solve thermal boundary, NITF or CHT should be used since SPF and HT cannot solve this. NITF and CHT are preferably used when investigating heat transfer in both the solid and fluid

instead of combining heat HT and SPF since the calculations will be faster and the settings are simpler.

4.5 Solver

When using turbulent flow k-ε it is possible to choose between direct solver and iterative solver. Per default iterative solver is given by the software for large models. This is a good solution for very large meshes, approximately more than 1miljon elements. For each iteration two or three iterations are also made with a coarser mesh. The drawback is that iterative solver is sometimes less robust then direct solvers. For smaller meshes a good way could be to change to direct solver. This will give a faster and possibly a more accurate solution but it consumes much more memory on the computer. The memory requirement for a direct solver is somewhere between $N^{1,5}$ and N^2 while the iterative solver scales as N where N is the number of degrees of freedom of the model[5].

4.6 Turbulence

When solving turbulent flow it´s good to have the data for the turbulence variables. If those are not available then rough approximations can be made for k and ε by COMSOL with equation (23) and (24)

$$k = \frac{3}{2}(|U|I_T)^2 \tag{23}$$

$$\varepsilon = C_\mu^{3/4}\frac{k^{3/2}}{L_T} \tag{24}$$

where I_T is the turbulence intensity and L_T is the turbulent length scale. If I_T is around 0,1% then the intensity is low turbulence. Fully turbulent flows usually have intensities between five and ten percent. The turbulent length scale L_T is a measure of the size of the eddies that are not resolved. For free-stream flows these are typically very small (in the order of centimetre). The length scale cannot be zero because that would imply infinite dissipation. For specifying L_T there are tables with values for different flows that can be used [5].

4.7 Convergence plot

On all simulations a convergence plot is automatically created during the simulation when solving locally. However, when solving the simulations in the cluster it wasn't possible to see this afterwards. The plotted curve should be as smooth as possible and it should go down to a least 10^{-1} to give a reliable results. As can be seen in Graph 1a, the plot can have spikes in the beginning but is then smoothed out and ends around 10^{-3}. When the solutions diverge it can look like in Graph 1b.

Graph 1a-b: Graph *a* shows a converged solution and graph *b* shows a diverged solution

a)

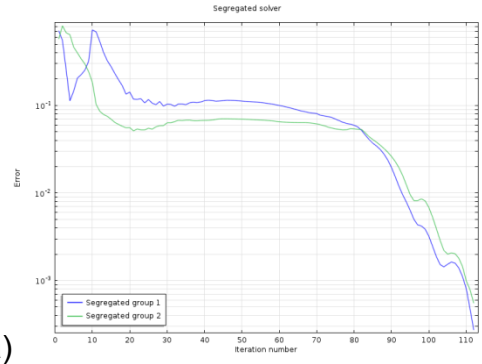

b)

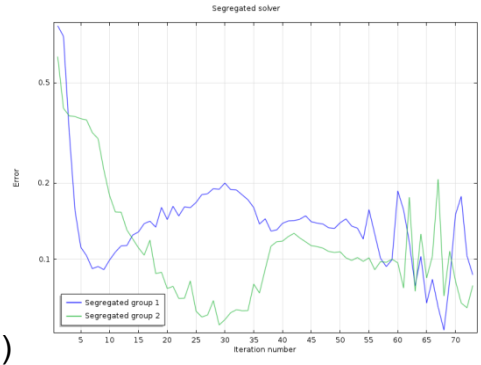

5 MEASUREMENTS

5.1 Machine data and test setup

To have a reference to validate computer simulations against, measurements was made on two 160 frame size[4] machines according to the IEC[5] standard. The first machine had a frame made of aluminium and was placed in a chamber as seen in Figure 9. The specifications of the machine can be found in Table 3. More information about this motor can be found in [7].

Table 3: Shows the data on the alumina frame

3-Motor M3AA 160 MLB 4			Cl. F	IP 55		
V	**Hz**	**kW**	**r/min**	**A**	**cos φ**	**duty**
400 Δ	50	15	1470	28,5	0,83	S1
690 Y	50	15	1470	16,5	0,83	S1
415 Δ	50	15	1473	27,7	0,82	S1

Figure 9: Machine 1 in test position

The second 160 machine was made of cast iron and was placed on test bench as seen in Figure 10. The machine was also used for other tests and was therefore connected with a machine on the DE. The fan on the machine on the right side is for this test removed to prevent influences on the air measurements done on the left machine. There were only cast iron machines available for this kind of test at the time of these measurements. The main difference between the cast iron and alumina housing relevant for these measurements is that the cast iron housing has higher and thicker fins. This freestanding arrangement was more suitable for the air flow measurements since the effects imposed by the box walls were removed.

[4] 160 frame size = 160mm from the lowest part oft he machine to the center of the axis
[5] International Electrotechnical Commission

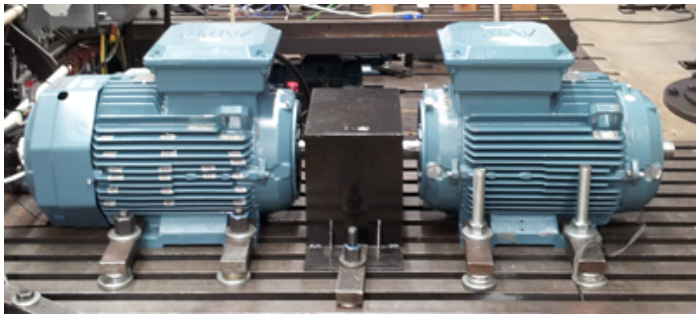

Figure 10: The machine on the left side was used for measurements.

The specifications for the cast iron frame motor are presented in Table 4. More information about this motor can be found in [7]

Table 4: Shows the data on the cast iron frame

3-Motor M4BP 160 MLB4			Cl. F	IP 55		
V	**Hz**	**kW**	**r/min**	**A**	**cos φ**	**duty**
400 Δ	50	15,0	1474	27,8	0,84	S1
690 Y	50	15,0	1474	16,1	0,84	S1
415 Δ	50	15,0	1477	27,0	0,83	S1

5.2 Air speed measurement

To measure the air speed distribution a Testo 400 instrument with a small hot bulb anemometer [8] had to be used to be able to get the anemometer in between the fins. This instrument shows only the velocity and not in what direction. The measure tip can be seen as the pen like part at the top of Figure 11. This was calibrated in 2006 and the protocol of the calibration can be found in appendix 5.

Figure 11: Testo 400 that was used for measuring air velocity

5.3 Measurement on alumina frame

These measurements were done early in the project to have a reference on what velocity one could expect and then use in the simulations. Measurements were done along five different fins at three different distances from the beginning of the fin relative to the fan cover. Measurements were performed on the following speeds: 100, 500, 1000 and 1500 rpm with no load

Table 5: Measure distance from the fan cover in centimetre in different ducts.

Duct	Measure point [cm]		
	Point A	Point B	Point C
Duct A	3		
Duct B	3	12	
Duct C	3	12	28
Duct D	3	12	28
Duct E	3	12	28

In Figure 12 one can see in which ducts the measurements have been done. Duct 1 and 2 is on the top of the machine. Blue duct D is symmetric to red duct E

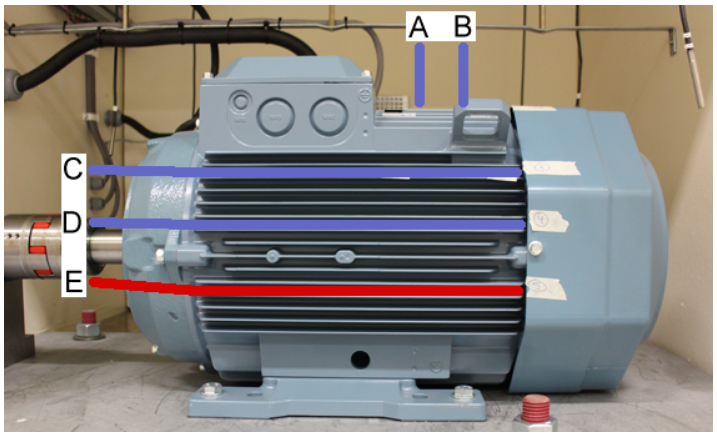

Figure 12: Shows in which ducts the measurements has been done.

Measure results from alumina frame

When increasing the rotational speed on the machine the air velocity increased even though the velocity decreased along the fins. This was expected but as can be seen in Table 6 the results in duct E gave unexpected results. The velocity did not increase as much as in the other ducts and also the air velocity increased along the fins instead of decreasing as in the other ducts. Therefore the measurement was done again later on in the project with a different setup and a cast iron frame machine.

Table 6a-d: Shows the measured air velocity [m/s] in different ducts and rpm

	Point 1	Point 2	Point 3
a)	100 rpm		
A	0		
B	0,25	0,13	
C	0,25	0,05	0,04
D	0,7	0,62	0,27
E	0,1	0,06	0,04
c)	1000 rpm		
A	0,26		
B	2,92	2,6	
C	5,25	1,95	1,57
D	8	6,54	4,95
E	0,45	0,54	1,98

	Point 1	Point 2	Point 3
b)	500 rpm		
A	0,05		
B	1,47	1,1	
C	3,2	0,88	0,6
D	3,9	3,22	2,41
E	0,17	0,26	0,91
d)	1500 rpm		
A	0,42		
B	4,8	3,6	
C	6,7	2,68	2,24
D	11,3	9,2	7,35
E	0,7	0,6	2,8

5.4 Measurement on cast iron frame

These measurements were made at the end of this work and therefore it was performed a little bit different compared to when measuring on the alumina housing that was done in the beginning. From the previous results of the alumina housing it was known that it would not be relevant to measure at 100 rpm. Measurements were also only done on one side of the machine but instead measurements were made on more ducts. The measurements were performed with no load in the following speeds: ±500, ±1000 and ±1500 rpm. The room temperature was 22.6°C. When the machine was running in positive speed it was rotating clockwise seen from the drive end side and counter clockwise when running in negative speed. In Table 7 one can see the distance from the fan cover that the measurements were performed. Some points were not possible to measure due to the fin design. These are marked with a black box in Table 7.

Table 7: Measure distance from the fan cover in centimetre in different ducts.

Measure point [cm]				
	Point 1	**Point 2**	**Point 3**	**Point 4**
Duct A	3	15	24	
Duct B	3	15		28
Duct C	4	15		29
Duct D	5	15	24	29
Duct E	5	15	24	29
Duct F	4	15		30
Duct G	3	15		28

In Figure 13 one can see in which ducts the measurements were taken. Duct B, C and D that is marked with blue lines is symmetric to the lined ducts E, F and G

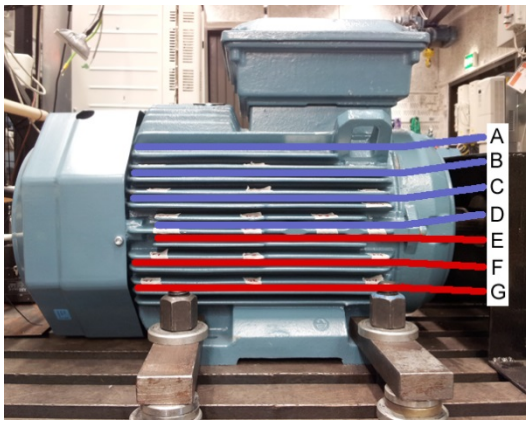

Figure 13: Shows in which ducts the measurements has been done.

Measure results from cast iron frame

Data related to ducts B and G are presented to illustrate the flow profile for the cast iron frame. The measured air velocity can be seen in Table 8. Since it can be difficult to notice a pattern from a table, the measured values from the first point in each rotational speed can also be seen in Graph 2

Table 8: Show the measured air velocity [m/s] on the cast iron frame

	Point 1	Point 2	Point 3	Point 4		Point 1	Point 2	Point 3	Point 4
	-500					+500			
B	2,05	1,3		1	**B**	2,1	1,6		1,2
G	2,9	1,7		1,15	**G**	2,15	1,25		0,8
	-1000					+1000			
B	4,1	2,8		2,35	**B**	4,05	3,4		2,75
G	4,5	3,5		2,6	**G**	4,5	2,85		1,8
	-1500					+1500			
B	6,75	4,4		3,55	**B**	6,8	5,25		4,4
G	6,8	5,65		4,15	G	7	4,3		3,05

Graph 2: Shows measured velocity in duct B and corresponding duct G

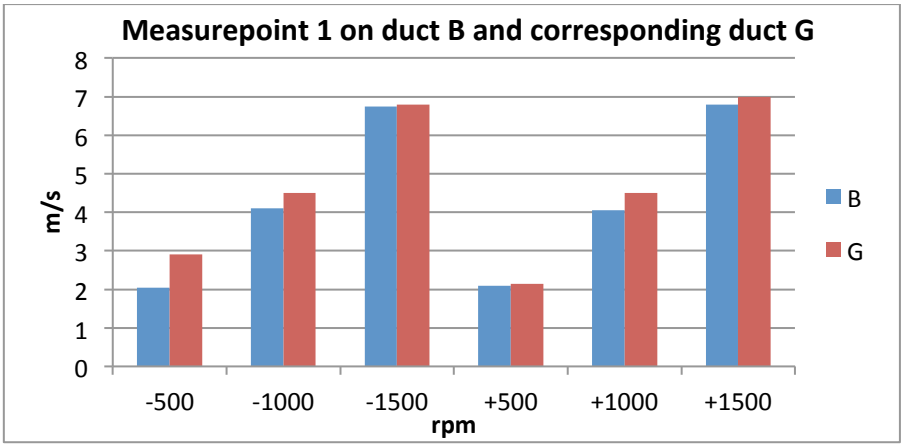

6 SIMULATIONS

6.1 Model

To be able to compare the efficiency of all the different designs it was important that they had the same basic conditions. Therefore one basic model was created first and then the airbox, heat plate and the base plate never changed in dimension. The outlet of the models had to be extended at least 10 centimetre after the fins. COMSOL has to solve the turbulence in the geometry that are created after the fins even though it is not be relevant for the results. This design which does not have any fins is used as a reference to be able to compare how efficient the fins on other models are versus no fin. These standard parameters can be seen in Table 9. This was important since otherwise the cooling surface and the heat distribution would change and give an impact on the results. When solving CHT an extra inlet domain was added to get a better convergence. Therefore this might differ on some of the pictures in this report depending on which geometry has been used as a reference.

Table 9: Shows the parameters that were used on most of the models

Parameter	Value
Distance between fins	0.010 [m]
Height airbox	0.075 [m]
Height frame	0.015 [m]
Height stator	0.003 [m]
Height fins	0.032 [m]
Length airbox	0.350 [m]
Length fins	0.320 [m]
Length air inlet	0.050 [m]
Length air outlet	0.100 [m]
Width total	0.036 [m]
Width of fins	0.003 [m]
Power losses in stator	120[W]
Air velocity at inlet	10[m/s]

This model can be seen in Figure 14 with the standard fins. Then position, shape and design of the fins were altered in many different ways to see if it is possible to improve the airflow and cooling. It was however not possible to increase the height of the airflow box too much because then COMSOL could not solve it. This is most likely because there will get both laminar and turbulent flow in the air domain.

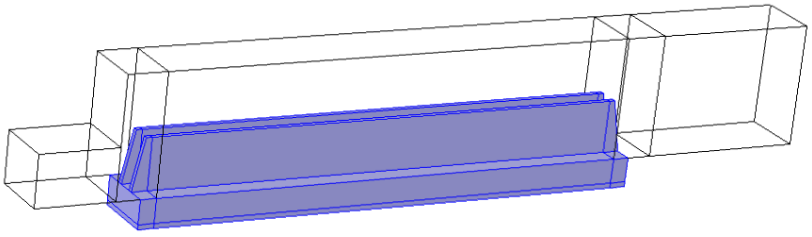

Figure 14: Shows the standard base plate with a standard design of the fins

6.2 Mesh

On models where the shape was uniform in the middle of the fins, the mesh was created with free triangular and then swept along the uniform fins and also along the outlet. This can be seen as the red areas in Figure 15. On the models that have an extra inlet this domain is also swept.

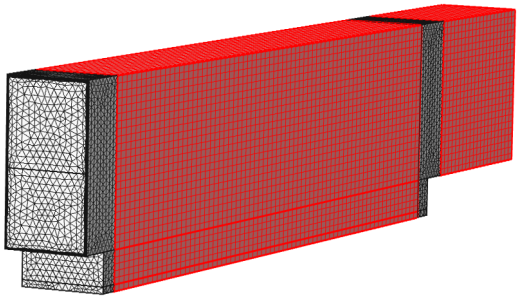

Figure 15: Shows in what domains the mesh is swept

The remaining domain was meshed with a free tetrahedral. If the shape on the fins was not uniform it was not possible to sweep the mesh and instead the free tetrahedral was used on all domains except for the outlet (and inlet). On all of the surfaces in the air domains a boundary layer was created. This can be seen as thin layers closest to the surfaces in Figure 16.

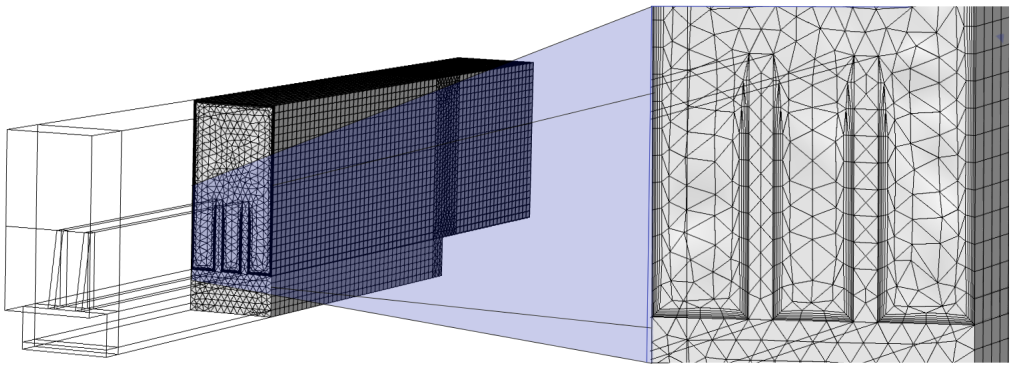

Figure 16: Shows the boundary layer on the surfaces of the air domain in a cut of the mesh model.

This is only used when solving SPF and CHT. When solving heat transfer, boundary layer could not be used since it only caused simulation errors. Therefore there was one mesh created for fluid flow and one mesh for heat transfer. On models that had smooth and straight fins the mesh element size was calibrated for fluid dynamics and set to fine. However when the shape of the fins was altered it was in most cases necessary to increase the resolution to finer to be able to solve the design. This on the other hand increased the solving time from approximately 3 hours to more than 2 days in the cluster. When solving CHT, a coarser mesh was used due to lack of time. For those fins that were not straight or did not have a smooth surface the free tetrahedral mesh were used along the entire fins. In section C in Figure 17 a coarse mesh is used along the fins. In section B and D which is the beginning and end of the fins, a finer tetrahedral mesh was used since that part of the fins will have a rather big impact

on the airflow. The inlet and outlet was still designed with swept mesh as can be seen as section A and E.

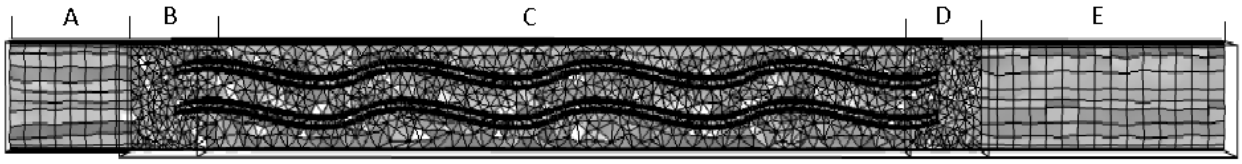

Figure 17: Section A and E shows the swept mesh of the inlet and outlet. Section B and D shows a finer mesh in the beginning and end of the fins. Section C uses a coarser mesh with free tetrahedral along the fins.

6.3 Turbulent flow K-ε (K-epsilon)

When adding the physic turbulent flow K-ε it was also necessary to define some extra conditions. The inlet was specified as the green boundary as can be seen in Figure 18 and the outlet was specified as the blue boundary.

Figure 18: Green boundary is inlet. Blue boundary is outlet

There was also symmetry added which is marked with red boundary in Figure 19. Since the bottom plate has a fixed width and the distance between the fins can vary on some models there is seldom real symmetry since the distance between the two fins and the distance between the fins and the walls are not the same. However when adding the symmetry feature in the models it was easier for the software to solve the models

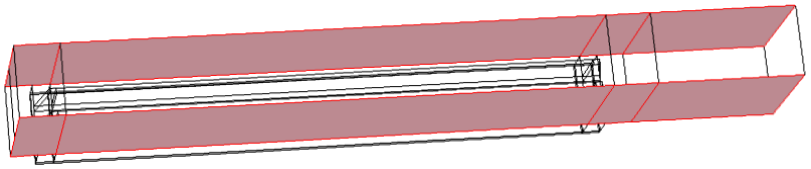

Figure 19: Symmetry boundary is marked with red

There were also some changes that had to be made in the settings of the features. These settings can be seen in Table 10.

Table 10: Changed settings in Turbulent flow K-ε

Feature	Main title	Subtitle	Droplist value	Entered value	Note
Fluid properties	Model inputs	Temperature	User defined	T0	=Parameter
Fluid properties	Model inputs	Absolute pressure	User defined	1[atm]	
Inlet	Velocity		Normal inflow velocity	U_in	=Parameter

6.4 Heat transfer in solids

There were also extra features added in Heat transfer in solids. Thermal insulation can be seen as blue boundary in Figure 20. On the sides of the models symmetry is used both in the fluid and the solid domain.

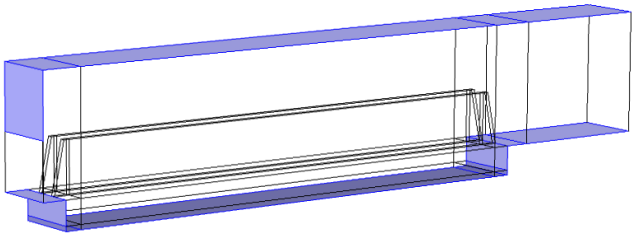

Figure 20: Thermal insulation marked as blue boundary

As a heat source the bottom plate with parameters taken from a silica glass library is used as seen in Figure 21.

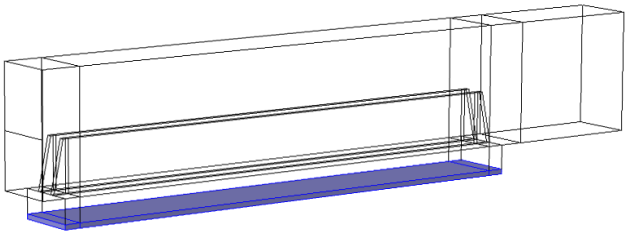

Figure 21: Heat source marked as blue domain

Between this heat plate and housing there is a thermal contact. The data for this is very difficult to get an exact number of as can be read at page 20. Therefore this contact data has been taken from a tutorial model in COMSOL. The air will transport heat away from the fins so the feature heat transfer in fluid is also added. The inlet and outlet has also to be defined the same way as in section 6.3.

6.5 Conjugate heat transfer

For the CHT models the material thermal grease was added between the stator and the frame. This was because it was easier to create the models since there was less parameters that had to be specified for the contact between stator and frame. There were more heat produced in the models because of lower thermal resistance but since all models that were compared hade the same settings they all had the same preconditions. In CHT the settings are similar as in SPF and HT. Symmetry was however not used in these models, instead the sides were considered to be walls with no slip. The features that were added/changed from the default setting can be seen in Table 11.

Table 11: Features that was added/changed from the default setting in CHT

Conjugate heat transfer			
Parameters			**Value**
Fluid	Dynamic viscosity	μ	mod1.mat3.def.eta(T[1/K])*param2
Initial values	Initial values	T	T0
Heat source	Heat source	W	q1/param
Inlet	Boundary condition	L_T	0.07*L_AI
Inlet	Velocity	U_0	U_in
Outlet			
Temperature	Temperature	T_0	T0
Outflow			
Thin Thermally resistive layer	TTRL	d_s	50[um]

If the step between the initial values and the final value is to big then the calculations might diverge. Therefore the continuation parameters param and param2 was created with the values 1000 100 1 and 10 5 1. Param is used to make the power losses and therefore the heat increase step by step and Param2 makes the viscosity decrease. This setting is found under the study node.

6.6 Simulations on a frame size 160 machine

As a reference, simulations was made on a CAD-model -model of an actual 160-machine. The CAD model is available at ABB:s webpage [9]. Since it is not possible to run a simulation on the entire machine[6], two fins were cut out from the machine. The fins chosen was located on the bottom of the machine and the cut out can be seen as a red box in Figure 22.

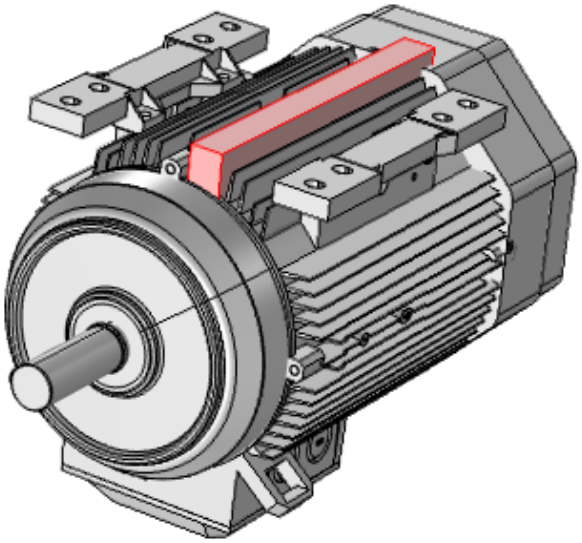

Figure 22: The red box shows what part that was used from the machine [9].

These fins were chosen because they were the ones most perpendicular to the housing and just plain fins without cuts or bumps. The inlet and outlet was

[6] The simulation is to complex and time consuming

extended because otherwise COMSOL was not able to solve the airflow. In Figure 23 one can see that the fins are not completely perpendicular to the housing and in Figure 24 one can also see how the inlet and the outlet is extended on the left and right side.

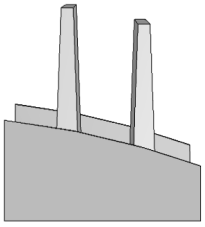

Figure 23: Shows the angle of the fins relative to the frame

Figure 24: Shows the fins from the side with the inlet and outlet on each side.

On this model, no heat simulation was performed since the geometry is not the same as in the other models and a comparison would therefore not be possible. The airflow simulation results are shown in Figure 25

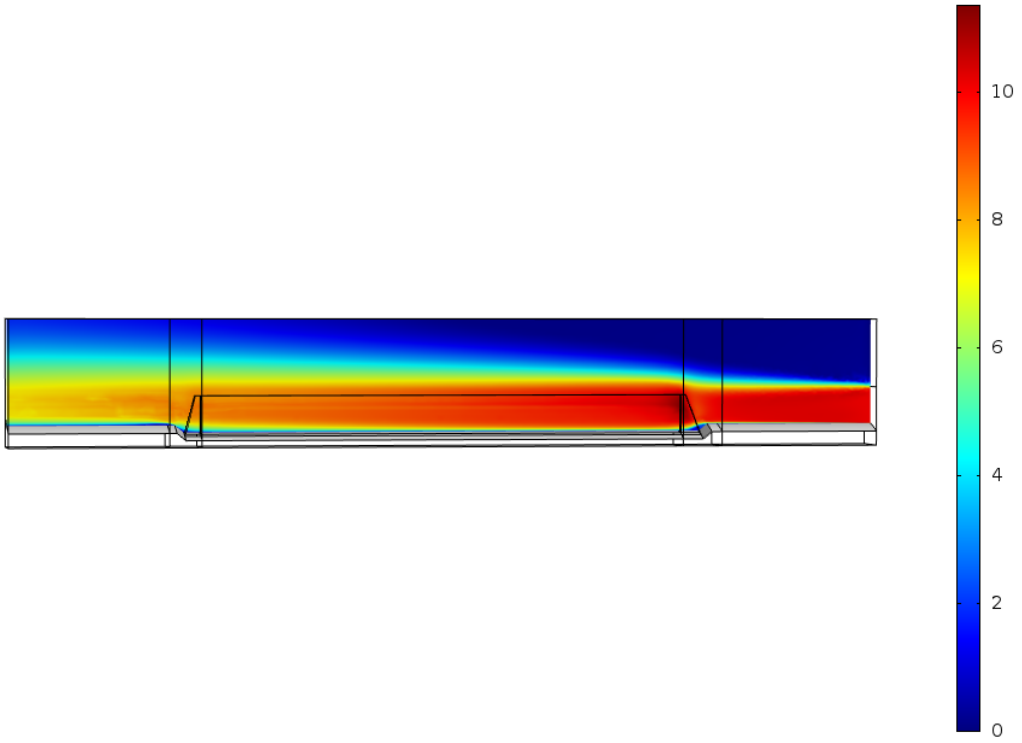

Figure 25: Air velocity between two fins on the geometry of a real machine.

6.7 Simulations on different designs

A lot of simulations had to be done before it was possible to get a model that was working regardless how the geometry and specifications was changed. In Table 12 the specifications that were changed in the different models are listed. Approximately half of the models have different shape of the fins then the straight and smooth fins that are normally used.

Table 12: Design information on the different models when using SPF. Yellow marks indicates changes

NR	Distance between fins (mm)	Height air space (mm)	Height stator (mm)	Height fins (mm)	Length of fins (mm)	Width fins (mm)	Power (W)	Air speed (m/s)	Material	Mesh notes	Fin shape design
1	10	75	-	32	320	3	-	10	Al	Fine	YES
3	10	75	-	32	320	3	-	10	Al	Finer	YES
4	10	75	-	32	320	3	-	10	Al	Finer	YES
5	10	75	-	32	320	3	-	10	Al	Finer	YES
6	10	75	-	32	320	3	-	10	Al	Fine	YES
7	10	75	-	32	320	3	-	10	Al	Finer	YES
8	10	75	-	32	320	3	-	10	Al	Fine	NO
11	10	75	-	32	320	3	20-50	10	Al, IC=Steel	Fine	NO
12.2	10	75-150		32	500	3	-	10	Al	Fine	NO
14	10	75	-	32	320	3	50-200	10	Al	Fine	NO
15	10	75	-	12-52	320	3	50	10	Al	Fine	NO
16	10-30	75	-	32	320	3	50	10	Al	Fine	NO
17	10	75	-	32	320	3	-	10	Al	Finer	YES
18	10	75	20	32	320	3	50-150	10	Al	Fine	NO
19	10	75	-	32	320	3	50-250	5, 10	Al	Fine	NO
20	10	75	-	32	320	3	20	10	Al	Finer	YES
21	10	75	-	32	320	3	20	10	Al	Custom	YES
22	10	75	-	32	320	3	20	10	Al	Custom	YES
23	10	75	-	32	320	1-5	20	10	Al	Fine	YES
24	-	75	-	-	-	-	20	10	Al	Normal	YES

When solving the models with CHT most of the same models were used as when solving for SPF with the exception of some minor changes and models that has been removed because they have been considered irrelevant from the results of the previous simulations. Also the numbering has changed. All the CHT models data can be found in Table 13.

Table 13: Design information on the different models when using CHT. Yellow marks indicates changes. Red marks indicates simulation that was not solved.

NR	Distance between fins (mm)	Temperature	Height fins (mm)	Width fins (mm)	Power (W)	Air speed (m/s)	Fin shape design
1	10	20	32	3	120	5, 10	NO
2	-	20	-	-	120	10	NO
4	10	20	12, 22, 32, 42, 52	3	120	10	YES
5	10	20	32	1, 5	120	10	NO
7	10	20	32	3	120	10	YES
8	10	20	32	3	120	10	YES
9	10	20	32	3	120	10	YES
10	10	20	32	3	120	10	YES
11	10	20	32	3	120	10	YES
12	10	20	32	3	120	10	YES
13	10	20	32	3	120	10	YES
14	10	20	32	3	120	10	YES
15	10	20	32	3	120	10	YES
16	10	20	32	3	120	10	YES

6.8 Results from CHT simulations

Temperature was evaluated in the centre of the frame. In Figure 26 it is possible to see the 16 different points were the measurements were done. This will show the heat distribution along the machine and also makes it possible to compare how efficiently the different designs will cool the frame.

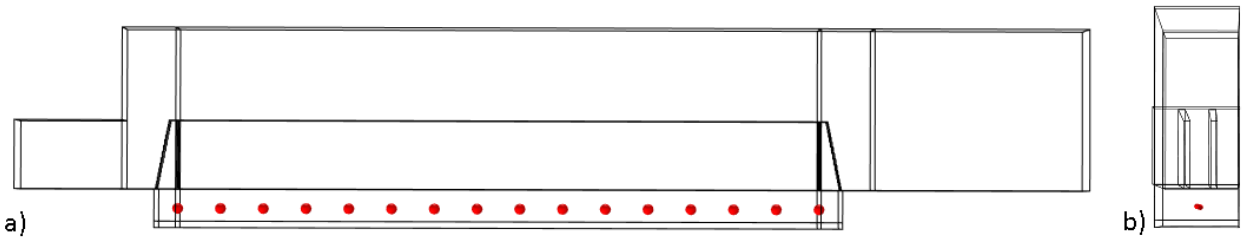

Figure 26a-b: Red dots indicate where the temperature was measured in the stator. The view in figure ***a*** is seen from the side of the fins and the view in figure ***b*** is seen from the inlet

In Graph 3 all the measured results are shown. The curve with the highest temperature is from simulation 1 where there are no fins. The second and fourth curve is when the height of the fins are 1.2 and 2.2 centimetre high. The third curve when the fins have the standard size of 3.2 centimetre but the inlet velocity is only 5 m/s. Since this temperature is approximately 50% higher compared to when the inlet velocity is 10 m/s at the same fins, it shows that it is important to get a high velocity of the airflow.

Graph 3: Shows the temperature along the center of the stator on different designs

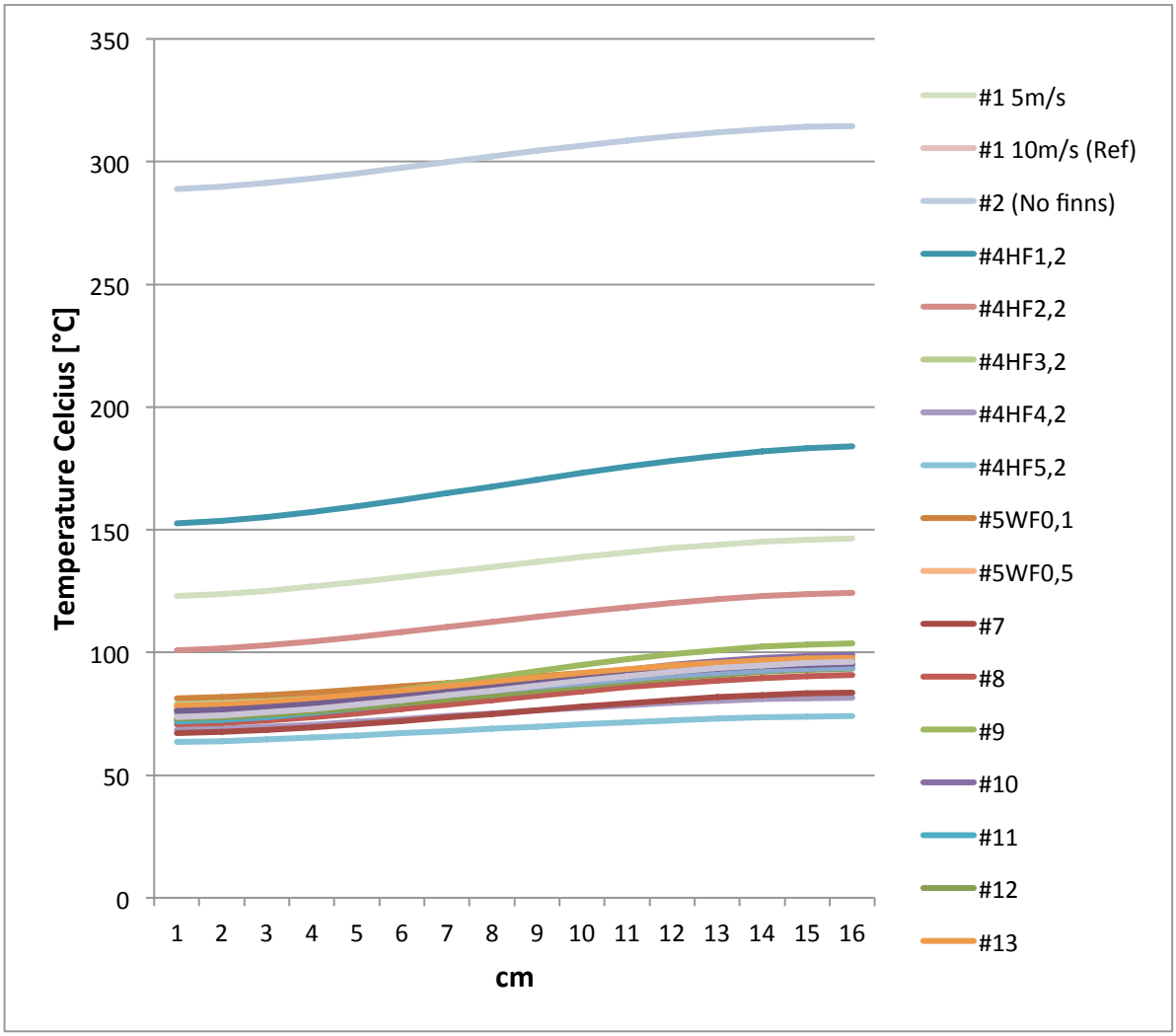

A selection of the designs with the lowest temperatures can be seen in Graph 4. Two of the curves with the lowest temperature have the fin height 5.2 and 4.2 centimetre. These are two of the most efficient designs that were simulated but these will also require more material which will lead to a larger and heavier machine. The third most efficient simulation is number seven, which has bars over the fins to prevent the airflow from deviate from the machine. The fourth most efficient design is number eight, which have tilted canals cut out from the fins. It makes a big difference on what direction those canals are tilted. If they are tilted in the opposite direction like in design number eight the air will deviate faster from the machine causing a very steep temperature rise along the machine

Graph 4: Shows the temperature along the center of the stator on the designs with the lowest temperature

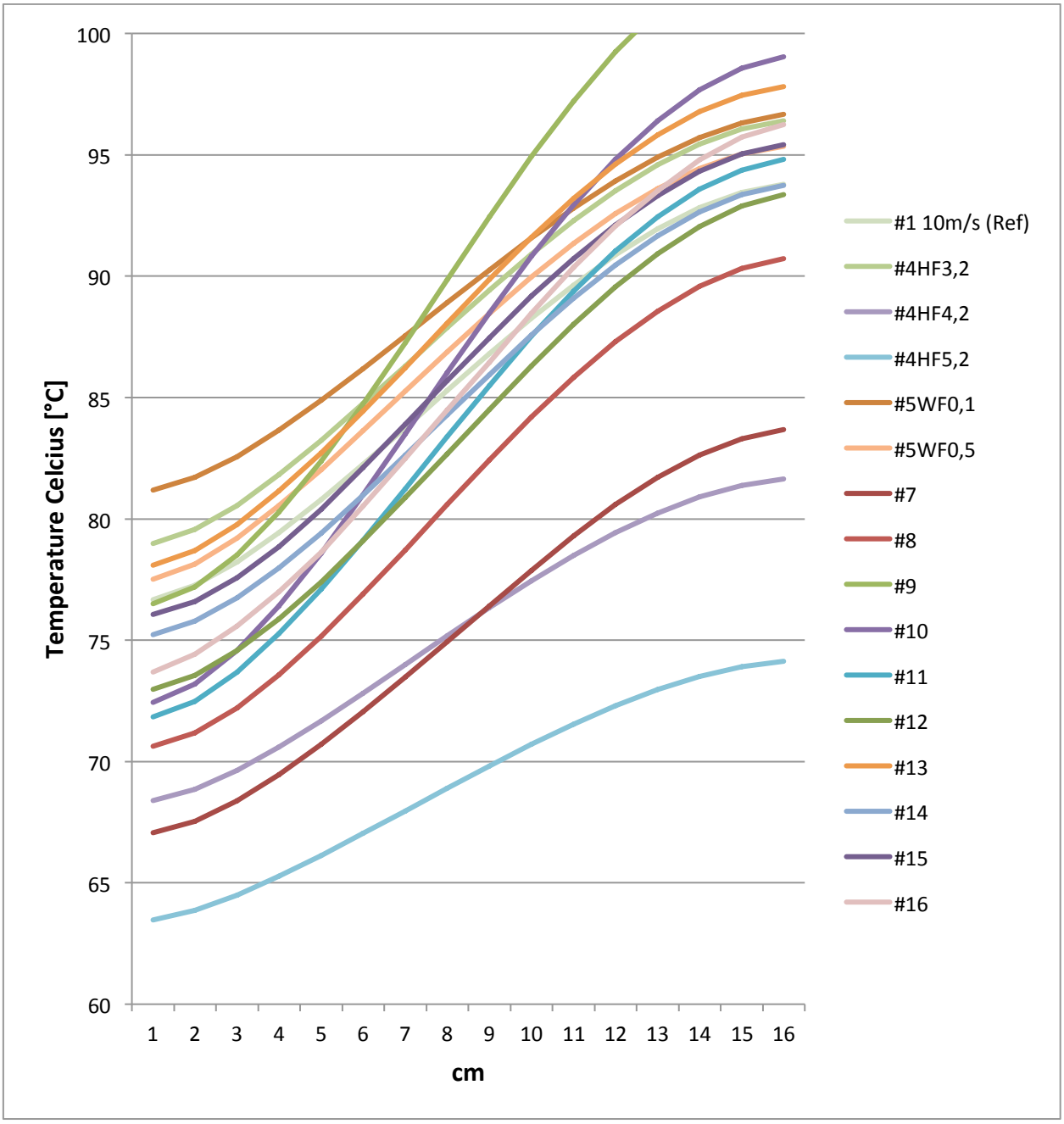

Pictures of heat transfer on the models can be seen in appendix 4. The slice of the air is in the middle between the fins and the surface temperature is shown on the fins and the stator.

The air velocity from the simulations can be seen in appendix 3. From those pictures it can be seen that the design of the fins has a large impact on how much the airflow will deviate

A comparison has been done on the temperature of the air in the middle between the fins. As can be seen in Graph 5, the air warms up much more along the machine when the air velocity is decreased from 10 to 5 m/s. This means that the

heat is not transported away from the fins with the same efficiency and since the surrounding air gets warmer so does the machine.

Graph 5: Shows the temperature of air in the middle between two fins at different velocities

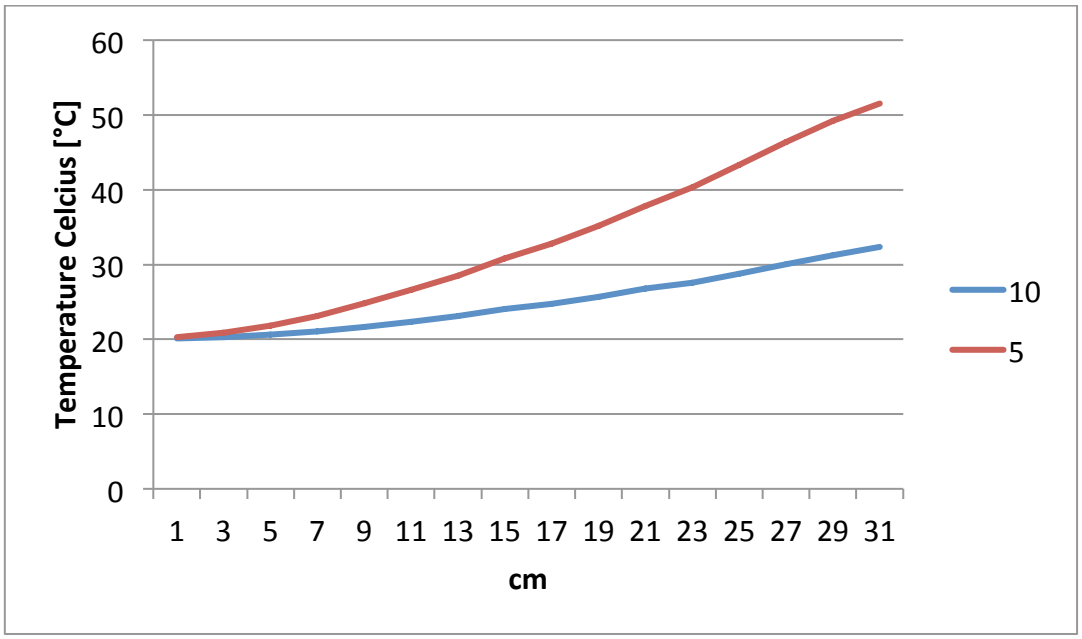

7 RESULTS

7.1 Airflow measurements and simulations

When air velocity measurements were done on the alumina frame, the highest velocity was measured to 11.3 m/s. Therefore the inlet velocity has been set to 10 m/s in the simulations.

Graph 6: Shows a comparison between simulated and measured velocity between the fins with an inlet velocity at 10 m/s

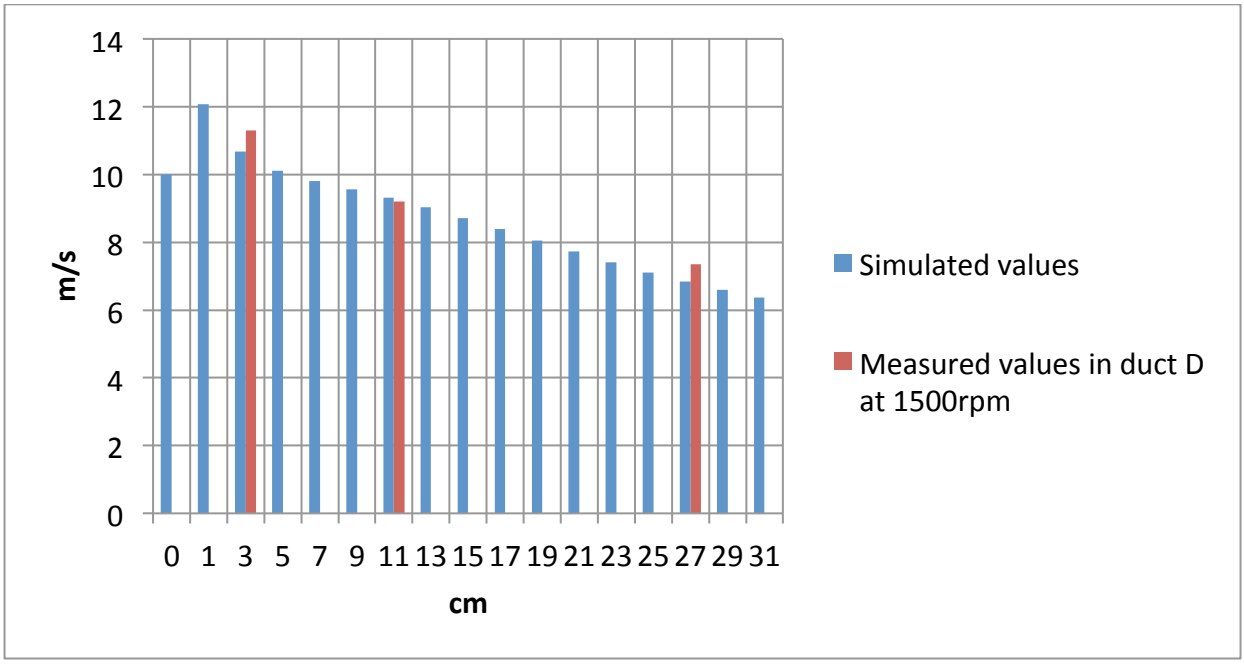

One simulation has also been done on the standard fin with an inlet velocity of 5 m/s to cover that velocity as well. There was no corresponding velocity measured on the machine so therefore two velocities has been used for comparison, where one is more and one is less than 5 m/s. The measured values are from duct *D* at rotational speed 500 and 1000 rpm as can be seen in Table 6.

Graph 7: Shows a comparison between simulated and measured velocity between the fins with an inlet velocity at 5 m/s

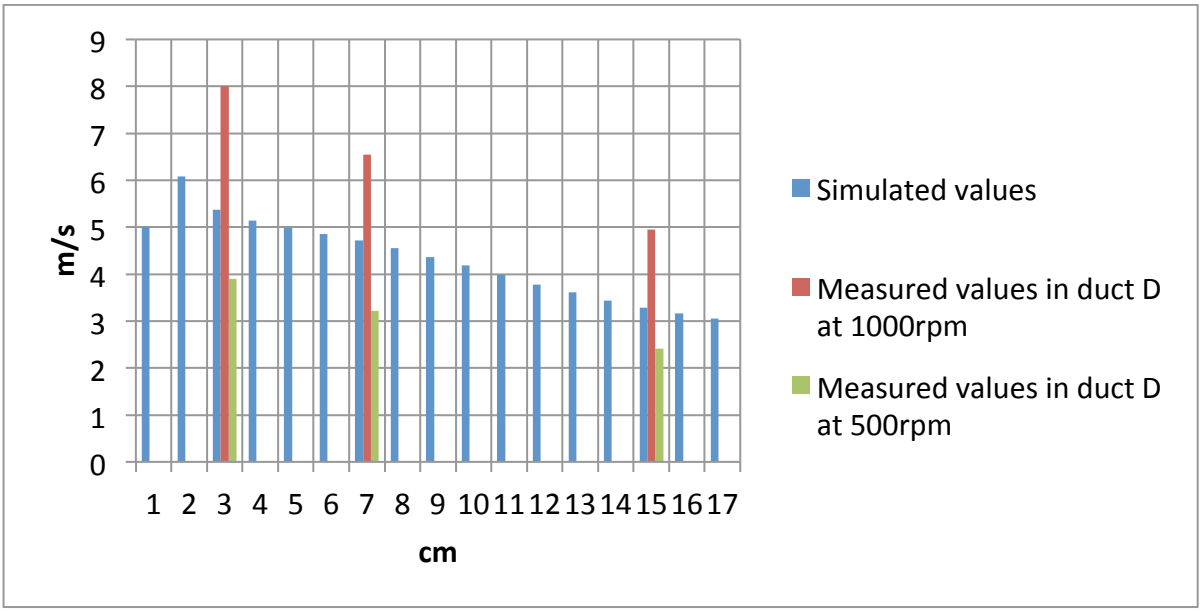

When comparing the measured values on that fin with the simulated values on a standard fin, one can see from Graph 6 and Graph 7 that the results are quite close to each other. It is however only measured in the middle between the fins so the measured and simulated values might differ more when getting closer to a surface.

7.2 Heat

The idea was to measure the temperature at steady state with a thermal camera. Since it takes several hours to reach steady state this was not possible because of lack of time. Also there had to be authorized personal running that test. Therefore thermal simulations could not be validated. Instead a thermal image [10] on a 6-pole IM (without flux optimizer) machine is used as a reference on how the heat is distributed. As can be seen Figure 27 there is a quite good cooling of the fins the first 10-20% from the fan but most of the machine is much warmer. Since it is the warmest part near the internal of the machine that sets the lifetime and power of the machine it is of importance to get a more even cooling distribution of the machine

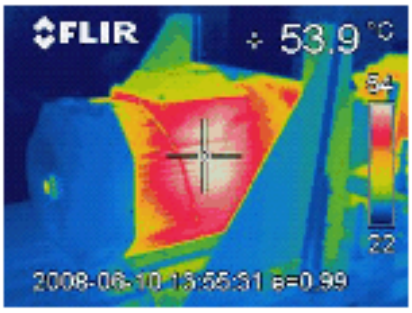

Figure 27: Thermal image of a machine with the fan mounted on left side [10].

8 DISCUSSION

8.1 Airflow measurements

The first measurements that were done were on an alumina frame. The results did not make sense at first since the velocity were close to zero in some ducts and was then increasing along the fin. Since the air probe does not indicate in what direction the air flows it was believed that those unexpected results were because the air was bouncing back from the chamber wall. To reduce this source of error, measurements were later done on a cast iron frame machine that was not placed in a chamber.

There were constantly small fluctuations in the results which were most likely because of the turbulent flow and that the measure probe was handheld which will give a small inaccuracy. The values that were noted were an average when measuring. After all the measurements had been done there was an extra measurement performed where the measure probe was fixed to a stand. Even then fluctuations were seen in the measurements, especially when using low speed in the machine. This time it was possible to notice that the fluctuations seemed to follow a pattern. This was however not investigated further.

8.2 The simulation models

The major part of the work in this thesis has been to understand the software and the physics needed to be able to solve the different designs that have been created. Even though the models do not seem that complex there were a lot of struggle to get the models working. The geometry that is used to simulate the design that is used on machines of today is a compromise. The height, length and width of the fins differ depending on what machine that is used as a reference and on what fin on the model the measurements is done. The dimension in the simulations is however considered to be a reasonable balance between the different geometries.

To simplify the simulations the fins were made rectangular in the cross section. If the fins would have been designed with a more triangular shape as on the actual fins, the heat transfer would have been improved (see Fin efficiency) but the geometry would be more complex and most likely causing longer computational time. Since rectangular fins were used in the simulations, velocity result on a standard fin might also differ slightly from the measured values on a machine

The paint on the surface of a machine would most likely reduce the heat transfer due to heat resistance but it was not possible to include this even though there was a function to include thin thermal layer in COMSOL. This was because the physical data of the paint was not found.

It is difficult to get physical data of the contact surface between the stator and frame on a machine (see Heat transfer in solids (HT)). Instead, when simulating CHT, thermal grease was used as contact medium. That improves the heat transfer from the stator but since all the models have the same settings this will make no difference for the results since it was only desired to see the difference of the heat convection between the models.

In the designs only two fins were used and the software considered the sides of the air box to be wall functions. There is a function in the program called periodic heat or flow condition that can be used when the design repeat itself which means that the left wall is equal to the right wall. This would have been extra useful on wave formed fins to get the right flow on both sides of the fins. One simulation was performed with this setting but the computational time was increased significantly so because of lack of time it was not possible to use this function in the rest of the models.

8.3 Sources of errors

In COMSOL it is possible to use either the COMSOL kernel or a CAD import module kernel for the geometry presentation. It is preferable to use the COMSOL kernel since it does not require an extra license but this could cause the error message “Internal error in geometry decomposition” in the geometry of some models. This can be solved by changing to the CAD import module kernel and then restart the program. It was not however investigated if the choice of geometry representation kernel had any impact on the results.

As mentioned (in Turbulent flow K-ε (K-epsilon)) K-ε might not be the best solver for this kind of problems since there will be a pressure drop when the air comes out from the inlet and in to the air box. It is however not mentioned how large the pressure drop have to be to have an impact on the result.

A rather coarse mesh was used on most of the models to save time when simulating. This might reduce the accuracy of the simulations but since the simulations are about a chaotic airflow it is almost impossible to get a perfect result that corresponds to reality.

Heat radiation has not been simulated even though it most likely will have an influence on the heat of the machine. All simulations consist of two fins and have almost the same geometry. Therefore it is unlikely that heat radiation will make a remarkable difference between the different designs but it is still important to be aware of its contribution.

8.4 Problems encountered during the simulations

There were problems that could not have been foreseen without knowing how the software solves the problems. For example when solving turbulent airflow it is sometimes necessary to extend the inlet and outlet more than what is interesting to see in the models. This is because COMSOL has to simulate if there is any airflow going back in or out of the model because of the turbulence. When the length of the inlet had to be changed so did the turbulence length to compensate for the length of the inlet. This was set to 0.7 times the length of the inlet.

The height of the air box could not be much more than 8 cm with the length of the models that were used. Otherwise the solution could not converge. This is most likely because the airflow would go from turbulent to laminar flow in some regions and then the k-ε function can’t converge. This will likely prevent the airflow from deviating as much as if it would have been completely open. It is possible to use something called “open boundary” that will let the air flow in and out of a boundary but this makes the simulations more unstable, takes more time to

compute and will make it more difficult to see how much heat that is transported away from the fins.

The first simulations were designed to be solved by the physics SPF and HT. When the results between different designs should be analysed and compared, it was desirable to see how much heat that was going out through the outlet compared to the inlet. The results that came from the simulations was not realistic so after some investigation it was found that the physics CHT should be used instead when simulating heat transfer in both solids and fluid. Despite that the desired results could not be retrieved. It turned out not to be as easy as it first might seem to get heat flux and convection results on a surface [5][11]. To get these kinds of results one has to have a very god understanding on the different physics and especially on how COMSOL solves the physical problems.

Two simulations had similar error messages that appeared a few minutes in to the simulations:

> "Error in user-defined function. -Function: ddmod1.mat3.def.rho_drho__T__internalArgument_drho__T__internalArgument"

This turned out to be a bug in the software and has been reported to be solved by COMSOL.

8.5 Future work

The results of velocity from the simulations have been compared with practical measurements on machines in the laboratory. However, to be able to verify if the simulations of the airflow is correct it might be necessary to use some kind of smoke that is transported along the machine, as in a wind tunnel test. This could also give a better understanding on what causes turbulent flow and where velocity losses are. One way to produce this kind of smoke is to use dry ice in a container with a narrow pipe and then pour a little bit of water over the ice which will cause a reaction. The smoke that comes out of the pipe can then flow along the machine. One of the advantages with dry ice is that is not harmful for neither the ones performing the test nor the environment.

9 REFERENCES

[1] H. O. Croft, *Thermodynamics, fluid flow and heat transmission*, First edit. Mcgraw-Hill book company, 1938.

[2] B. Appelqvist and D. Loyd, *Grundläggande teknisk strömningslära*. Ingenjörsförlaget AB, 1979.

[3] Y. A. Cengel, J. M. Cimbala, and R. H. Turner, *Fundamentals of thermal-fluid sciences*, 4th editio. Mcgraw-Hill book company, 2012.

[4] C. Nordling and J. Österman, *Physics handbook for science and engineering*. Studentlitteratur, 2009.

[5] COMSOL, "COMSOL multiphysics 4.3b (Help section)." 2013.

[6] A. Boglietti, "Thermal analysis techniques in electrical machines," 11061.

[7] ABB, "Low voltage Process performance motors according to EU MEPS," 2013. [Online]. Available: http://www05.abb.com/global/scot/scot234.nsf/veritydisplay/4926be1f5d4df488c1257bf7003aa496/$file/Catalog_Process_performance_acc_to_EU_MEPS_9AKK105944_EN 10_2013_LOW.pdf. [Accessed: 11-Nov-2013].

[8] Nordtec, "Varmkroppsgivare," 2013. [Online]. Available: http://www.nordtec.se/givare/varmkroppsgivare-0. [Accessed: 14-Oct-2013].

[9] ABB, "Processmotorer IE2, aluminium," 2013. [Online]. Available: http://www.abb.se/product/seitp322/2336d459db1a508cc12578b0003c841a.aspx?productLanguage=se&country=SE.

[10] R. Rajabi Moghaddam, *Synchronus Reluctance Machine (SynRM) in Variable Speed Drives (VSD) applications*. Stockholm: Universitetsservice, 2011, p. 253.

[11] COMSOL, "My flux calculation seems wrong," 2013. [Online]. Available: http://www.comsol.com/support/knowledgebase/973/. [Accessed: 14-Oct-2013].

10 APPENDIX

Appendix 1	Efficiency on different fin design (theory).
Appendix 2	Pictures of the different designs that has been simulated.
Appendix 3	Pictures of the airflow on the different designs.
Appendix 4	Pictures of the heat transfer on the different designs.
Appendix 5	Accuracy and calibration protocol of Testo 400

Appendix 1

Straight rectangular fin

$$m = \sqrt{2h/kt} \qquad \eta_{fin} = \frac{\tanh mL_c}{mL_c}$$

$$L_c = L + t/2$$

$$A_{fin} = 2wL_c$$

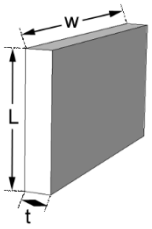

Straight triangular fin

$$m = \sqrt{2h/kt} \qquad \eta_{fin} = \frac{1}{mL}\frac{l_1(2mL)}{l_0(2mL)}$$

$$A_{fin} = 2w\sqrt{L^2 + (t/2)^2}$$

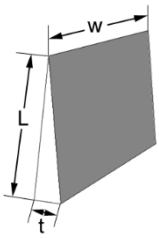

Straight parabolic fin

$$m = \sqrt{2h/kt} \qquad \eta_{fin} = \frac{2}{1+\sqrt{(2mL)^2+1}}$$

$$A_{fin} = wL[C_1 + (L/t)\ln(t/L + C_1)]$$

$$C_1 = \sqrt{1 + (t/L)^2}$$

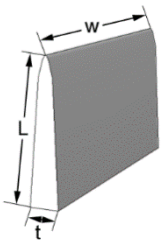

Pin fins of rectangular profile

$$m = \sqrt{4h/kD} \qquad \eta_{fin} = \frac{\tanh mL_c}{mL_c}$$

$$L_c = L + D/4$$

$$A_{fin} = \pi D L_c$$

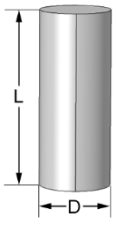

Pin fins of triangular profile

$$m = \sqrt{4h/kD} \qquad \eta_{fin} = \frac{2}{mL}\frac{l_2(2mL)}{l_1(2mL)}$$

$$A_{fin} = \frac{\pi D}{2}\sqrt{L^2 + (D/2)^2}$$

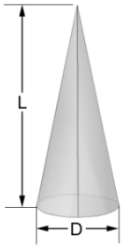

Pin fins of parabolic profile

$$m = \sqrt{4h/kD} \qquad \eta_{fin} = \frac{2}{1+\sqrt{(2mL)^2+1}}$$

$$A_{fin} = \frac{\pi L^3}{8D}\left[C_3C_4 - \frac{L}{2D}\ln\left({}^{2DC_4}/_{L} + C_3\right)\right]$$

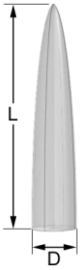

APPENDIX 2

These are the different designs that were simulated and solved. The simulation number is written below each figure. The numbers in parenthesis shows the number of the model when used for CHT simulations

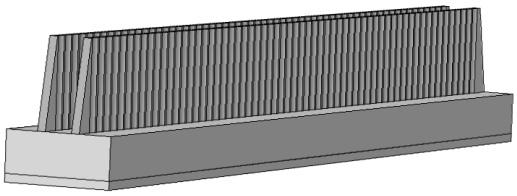

1, 3 (10)

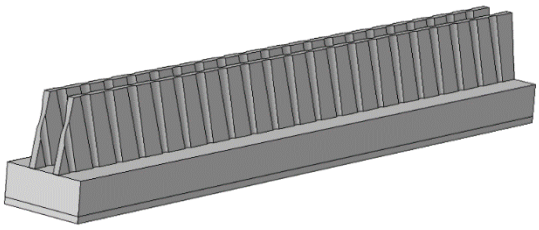

4 (9)

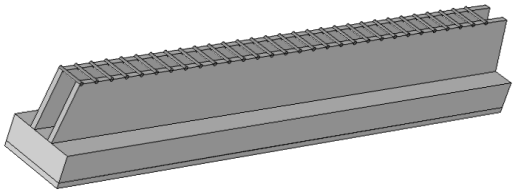

5, 6

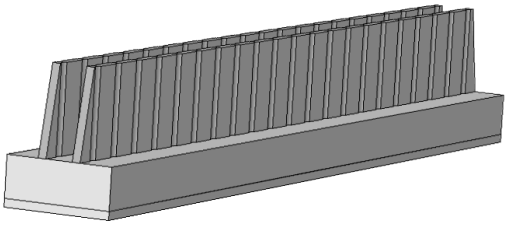

7 (11)

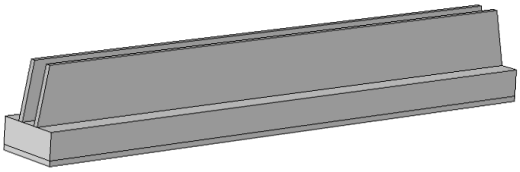

8, 11, 14, 19 (3)

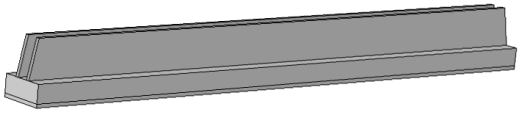

12

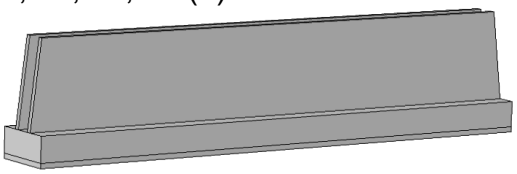

15 (4)

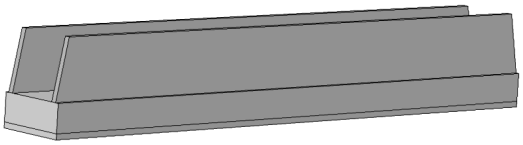

16 (6)

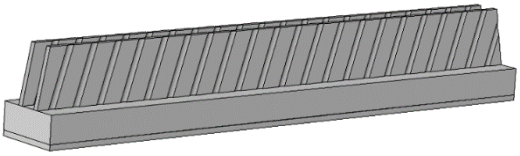

17 (8)

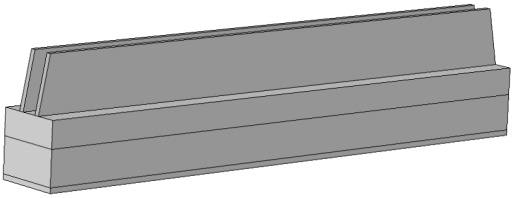

18

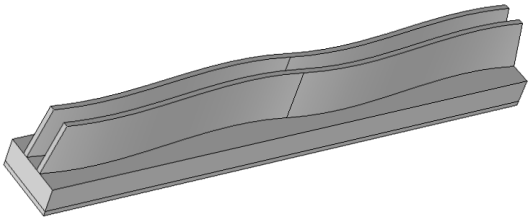

20 (13)

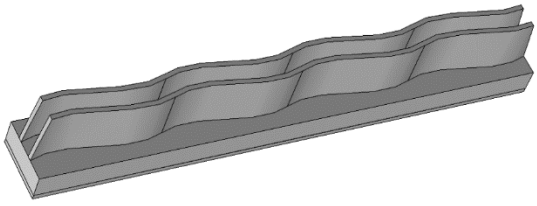

21 (15)

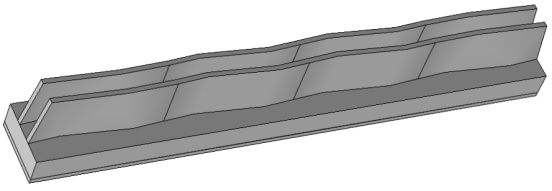

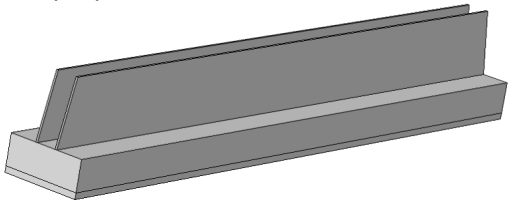

22 (14)

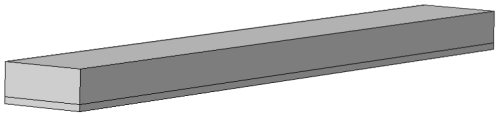

23 (5)

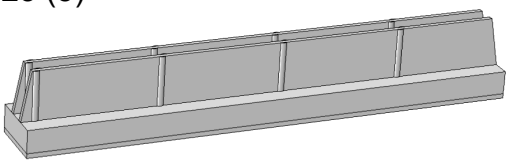

24 (2)

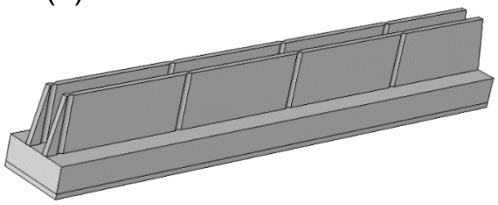

25 (16)

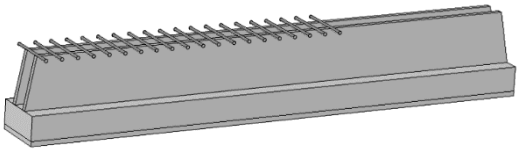

26 (12)

(7)

Appendix 3

Pictures of the airflow from CHT simulations. The coloured slice that shows the velocity in meters per second is in the middle between the fins. The number with an arrow pointing down in the lower left corner shows the lowest velocity that is simulated in the figure. The number with an arrow pointing up in the lower right corner shows the highest velocity that is simulated in the figure.

1) Standard fins (10m/s)

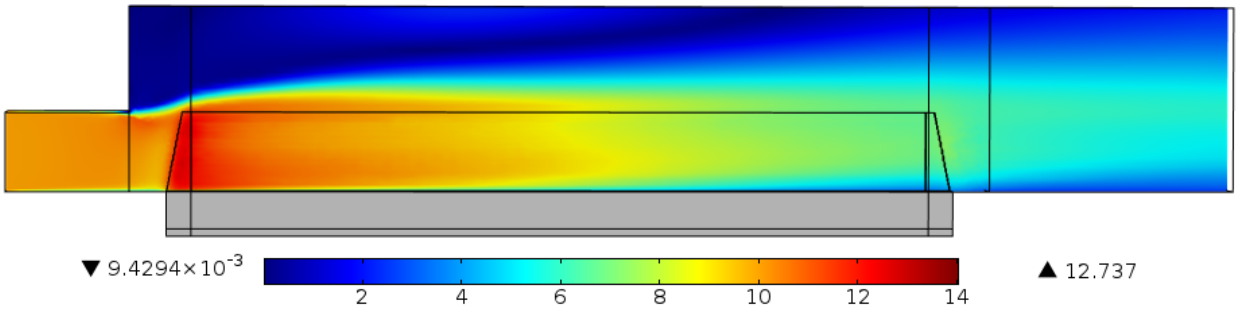

1) Standard fins (5m/s)

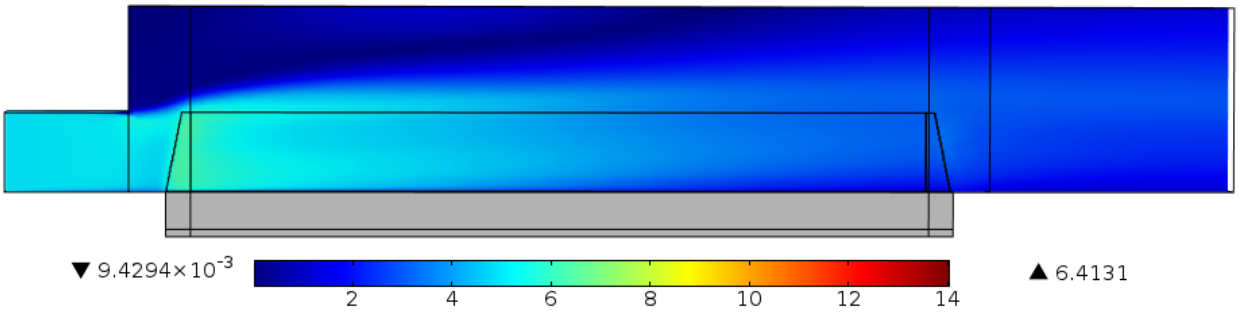

2) No fin

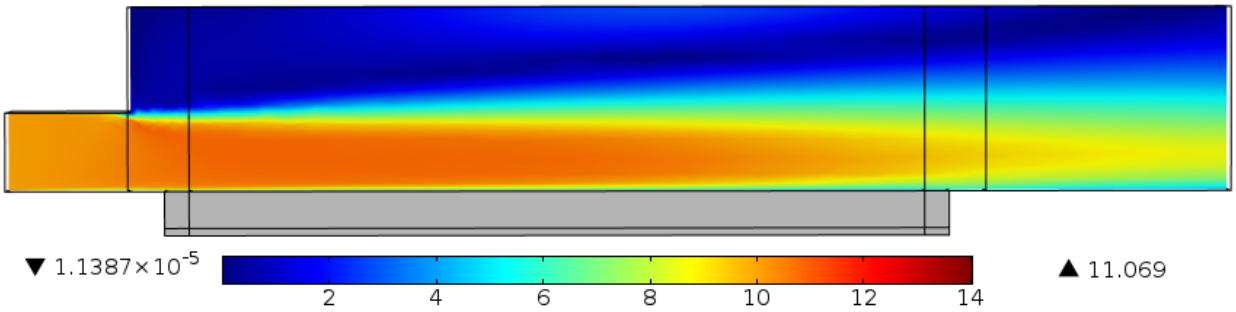

4) Fin height 12mm

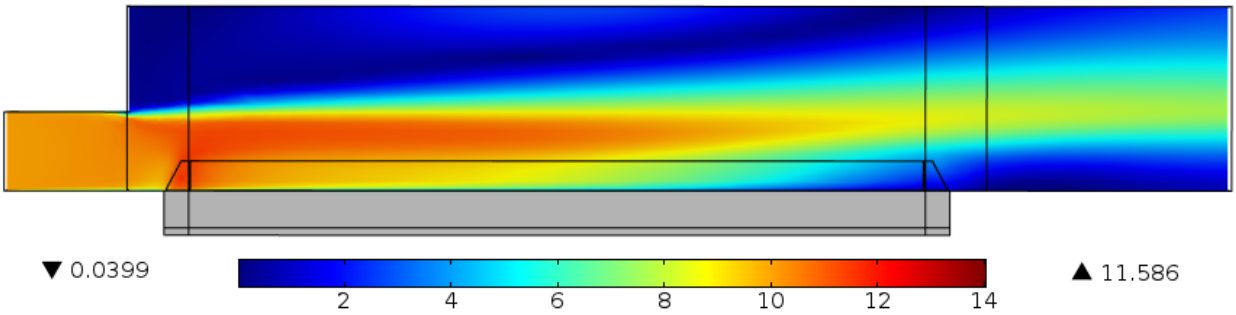

4) Fin height 22mm

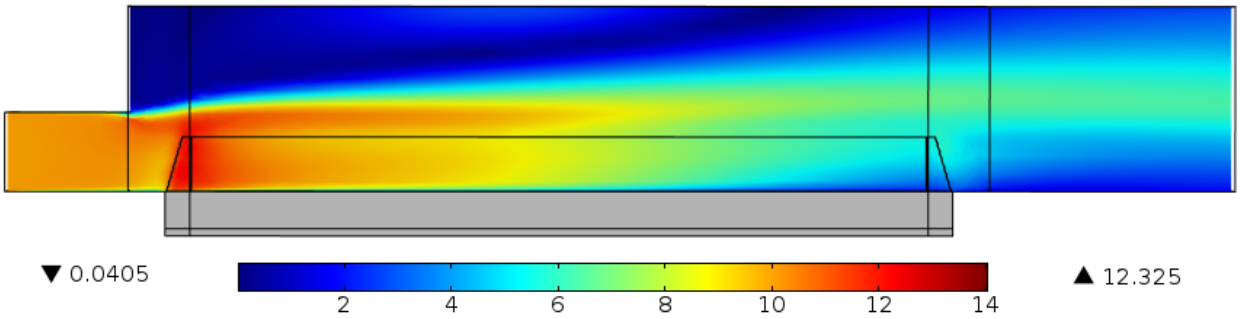

4) Fin height 32mm

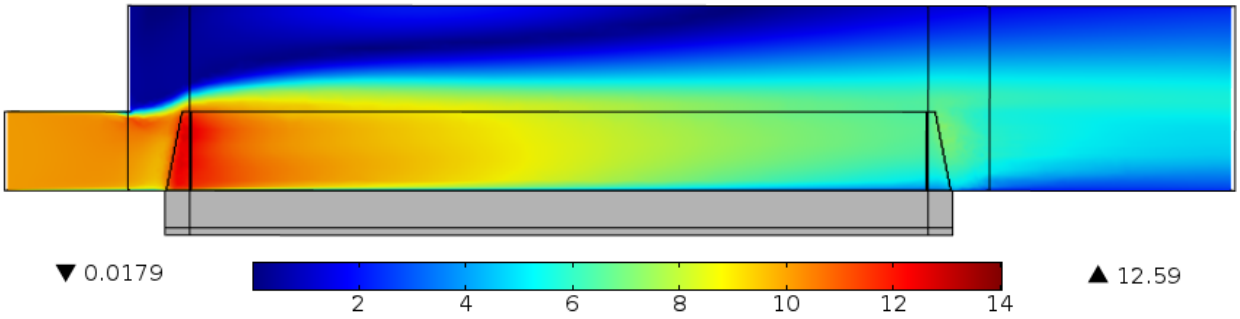

4) Fin height 42mm

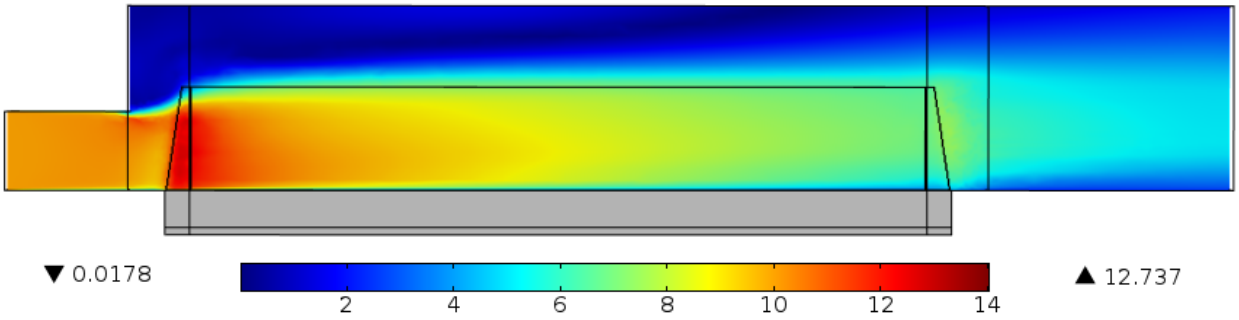

4) Fin height 52mm

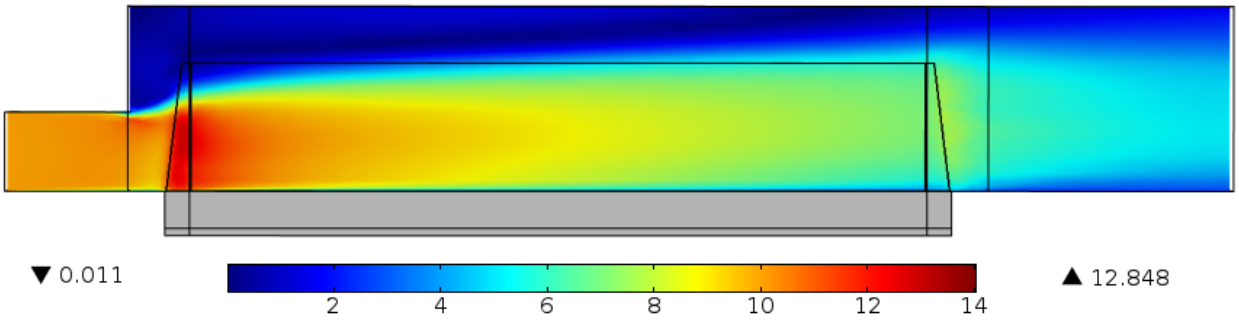

5) Fin thickness 1mm

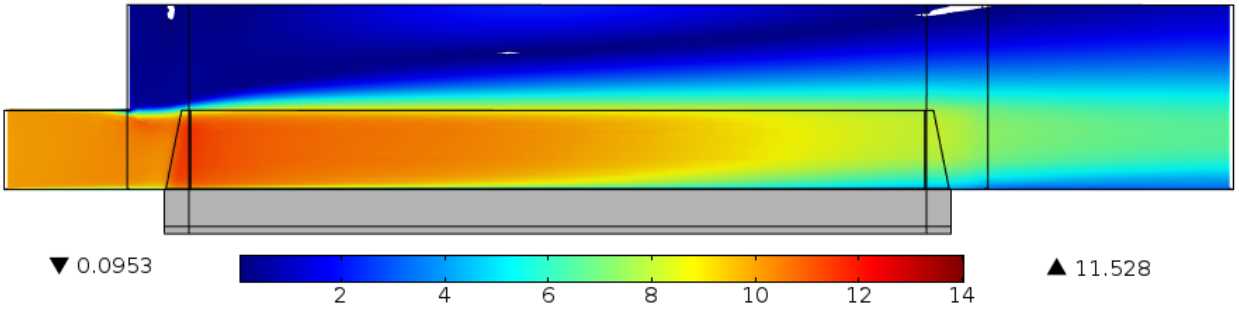

5) Fin thickness 5mm

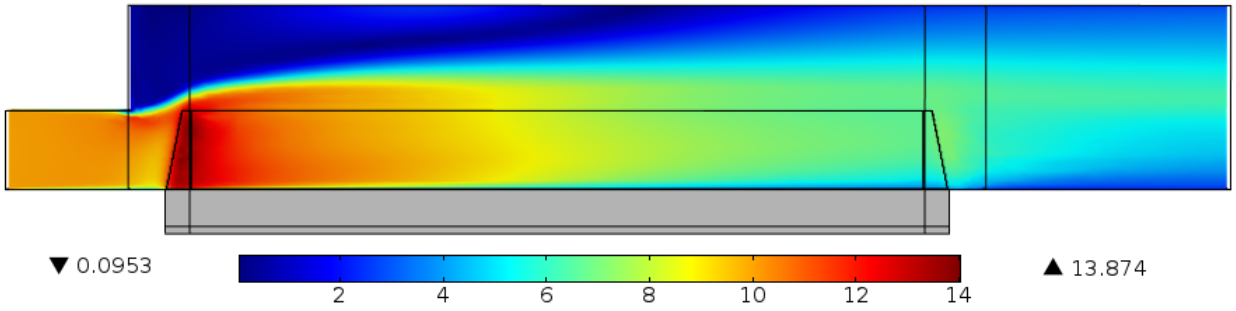

7) Bars

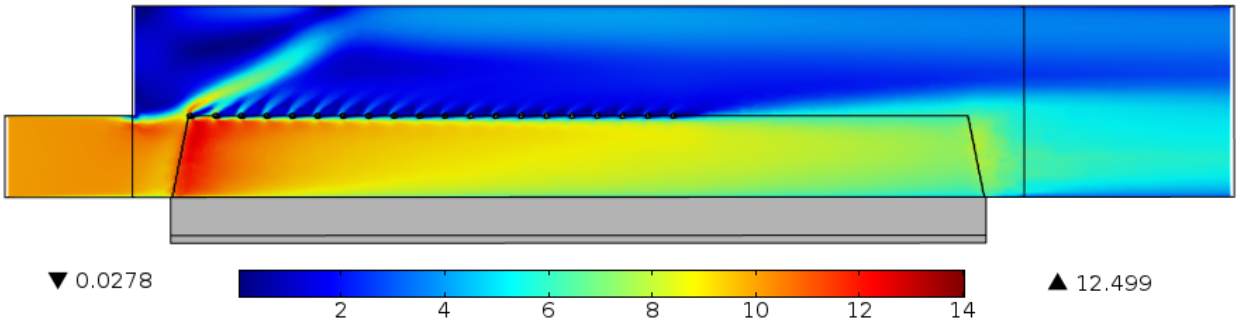

8)

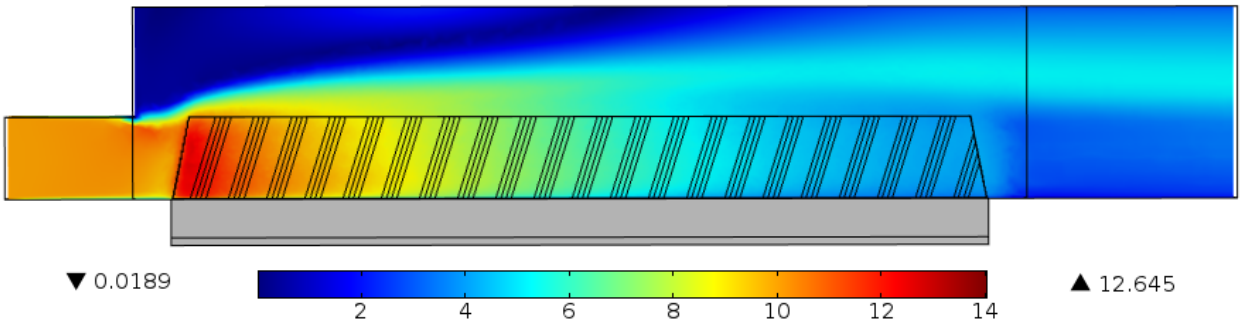

9)

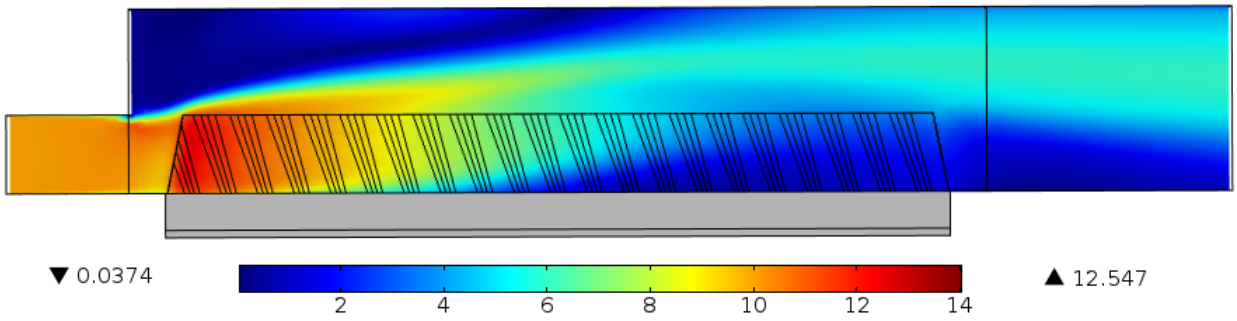

10)

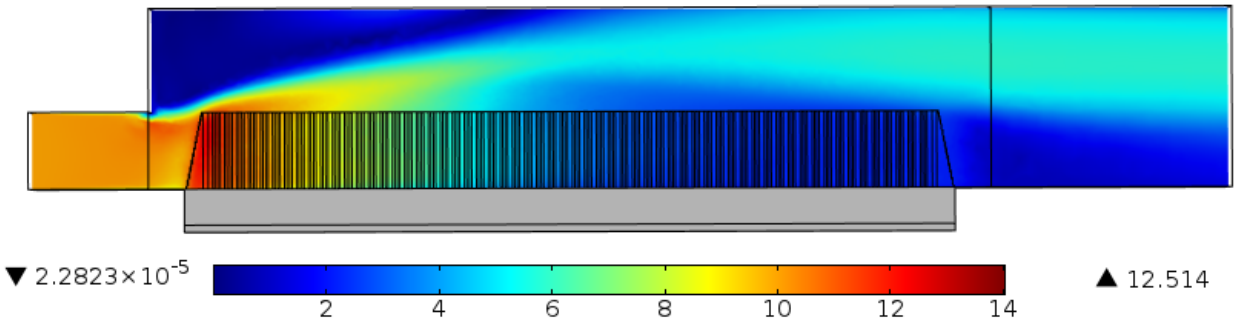
▼ 2.2823×10^-5
2
4
6
8
10
12
14
▲ 12.514

11)

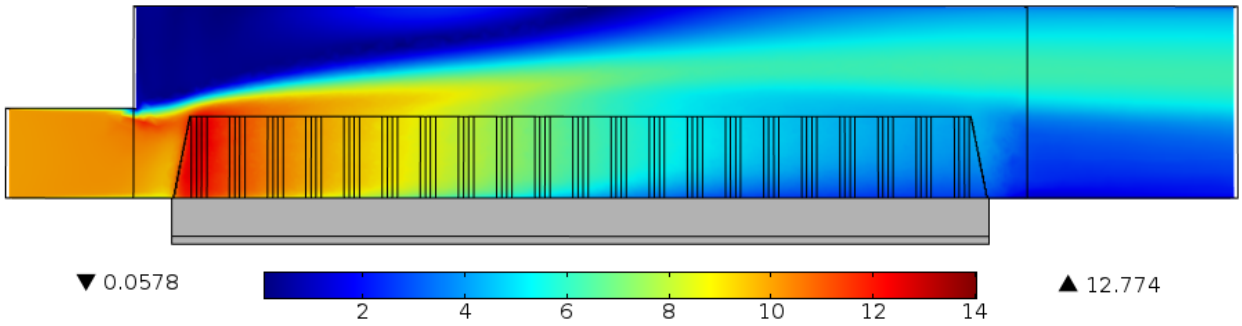
▼ 0.0578
2
4
6
8
10
12
14
▲ 12.774

12)

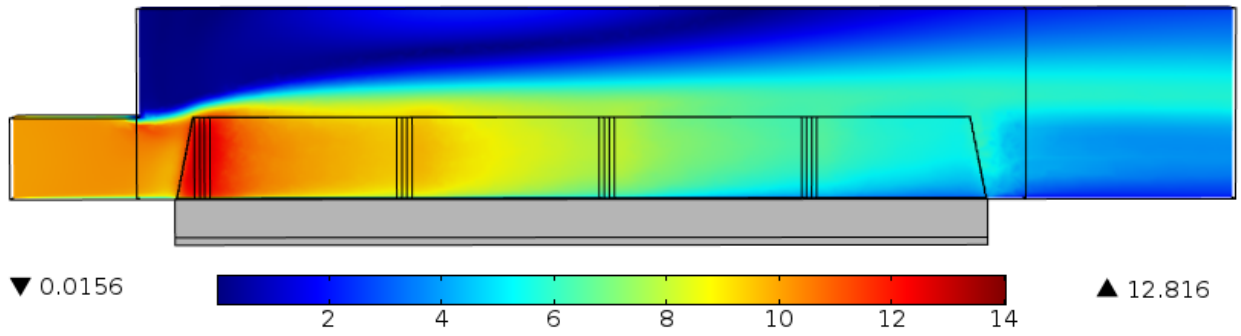
▼ 0.0156
2
4
6
8
10
12
14
▲ 12.816

13)

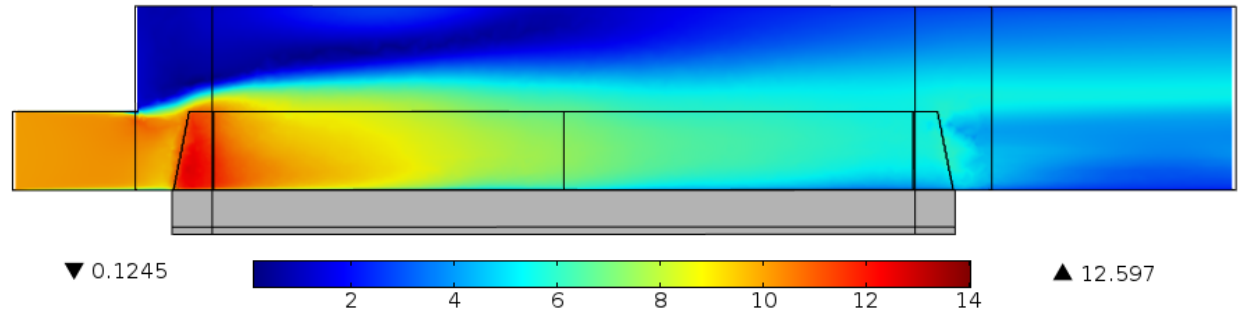
▼ 0.1245
2
4
6
8
10
12
14
▲ 12.597

14)

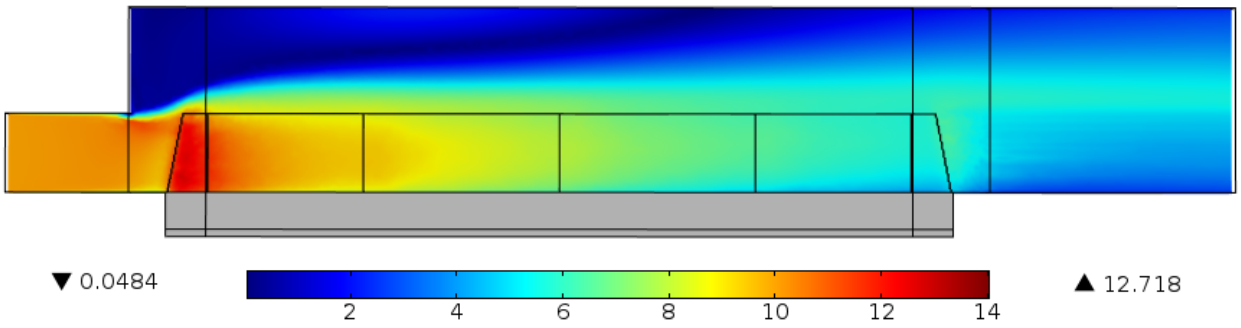
▼ 0.0484
2
4
6
8
10
12
14
▲ 12.718

15)

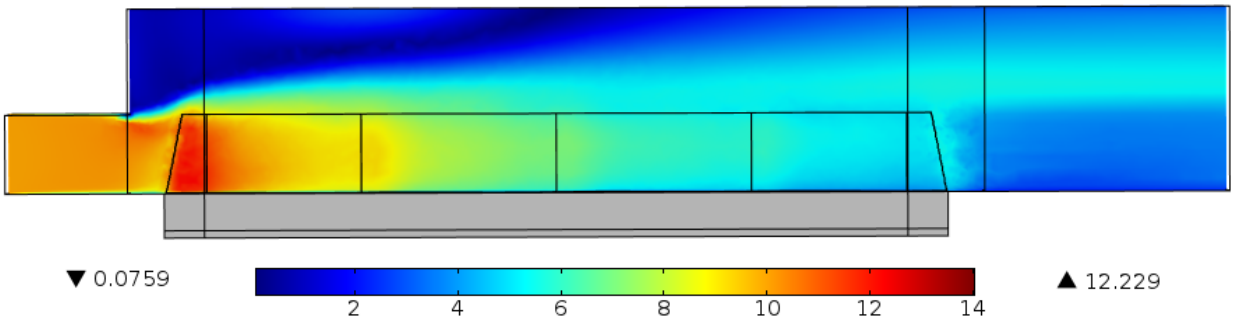
▼ 0.0759
2
4
6
8
10
12
14
▲ 12.229

16)

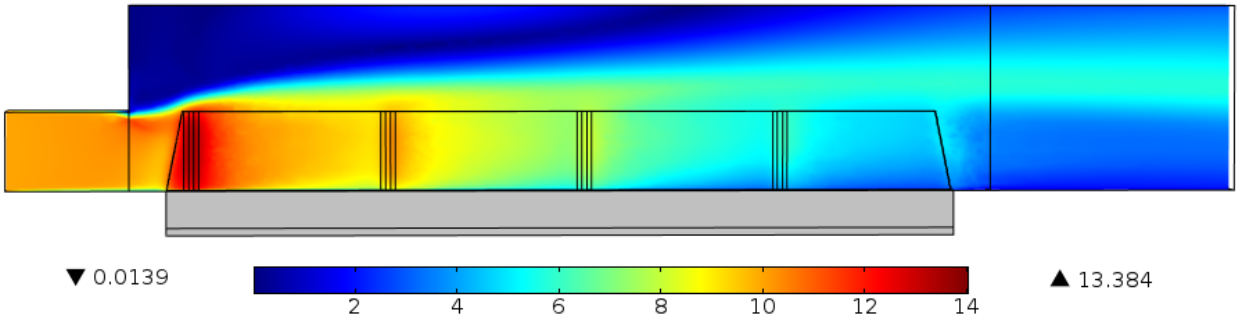
▼ 0.0139
2
4
6
8
10
12
14
▲ 13.384

Appendix 4

Pictures of heat transfer in air from CHT simulations. The slice of the air is in the middle between the fins and on the fins and the stator the surface temperature is shown. The temperature is measured in degrees Celcius. The number with an arrow pointing down in the lower left corner shows the lowest temperature that is simulated in the figure. The number with an arrow pointing up in the lower right corner shows the highest temperature that is simulated in the figure.

1) Standard fins (10m/s)

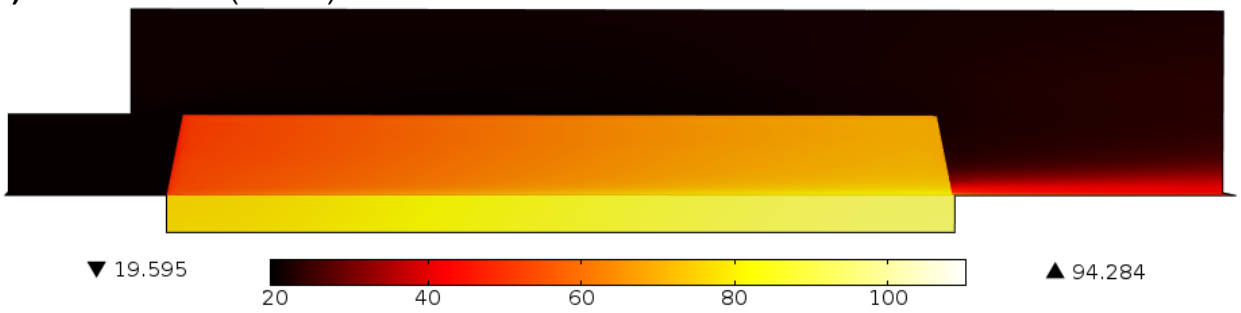

1) Standard fins (5m/s)

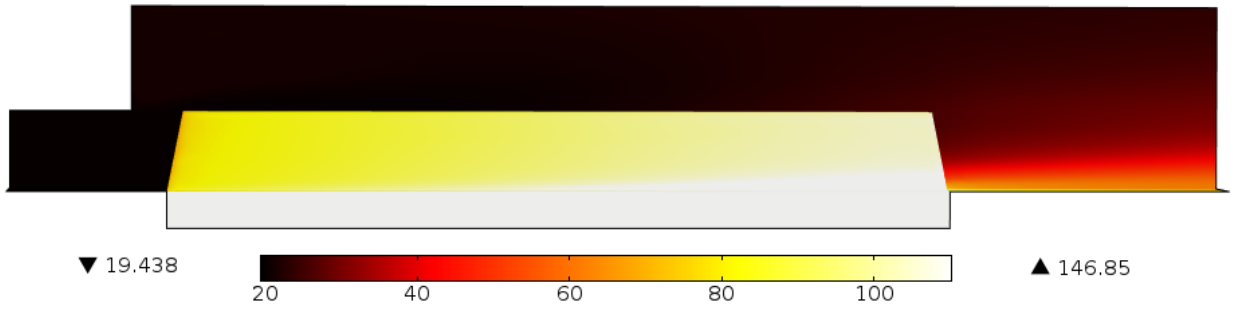

2) No fin

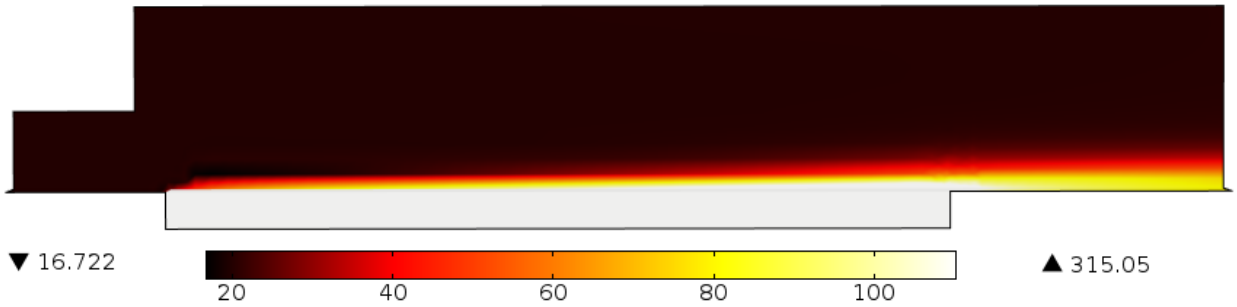

4) Fin height 12mm

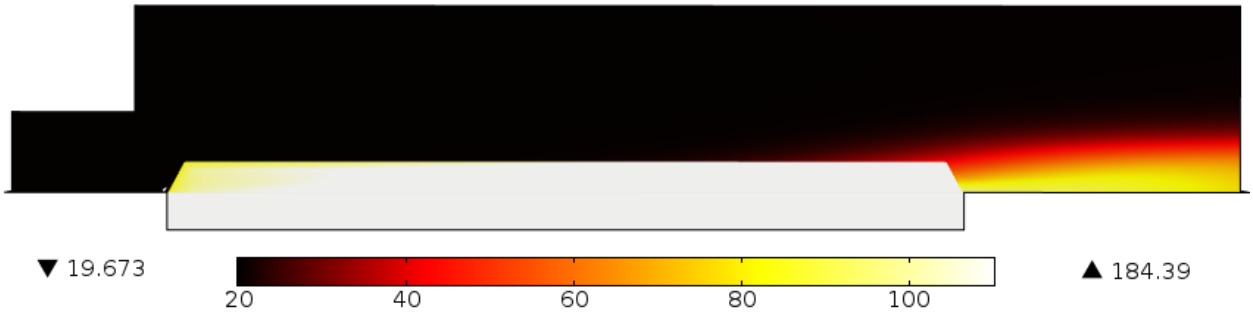

4) Fin height 22mm

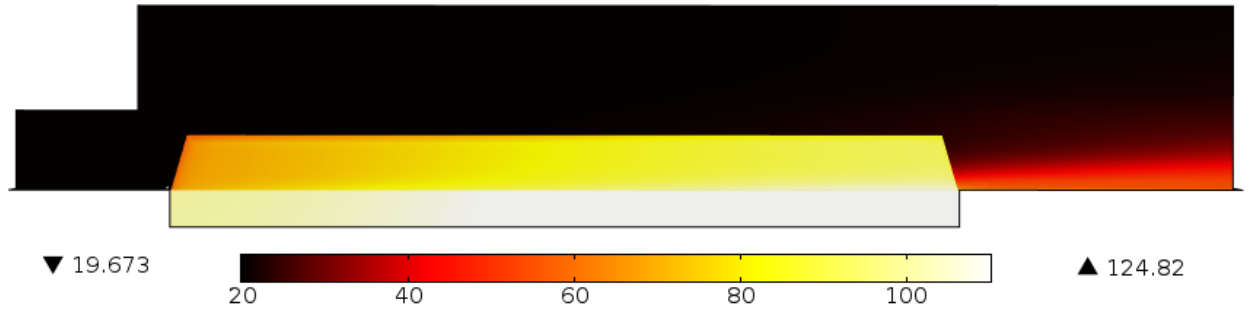

4) Fin height 32mm

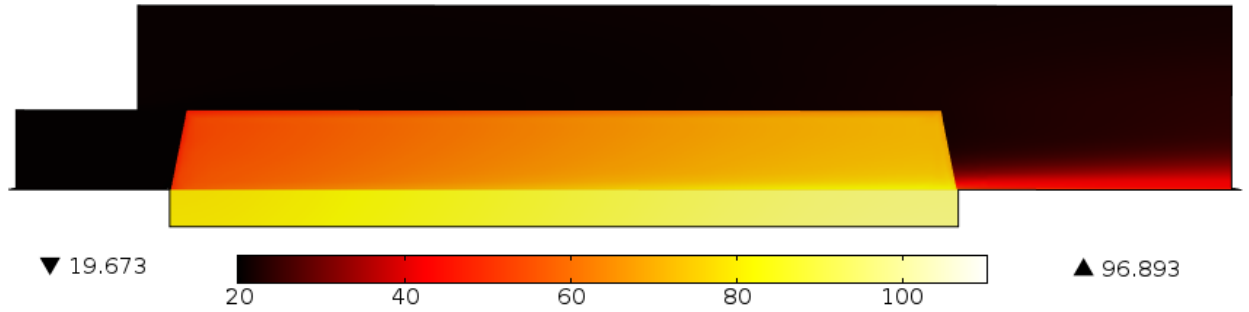

4) Fin height 42mm

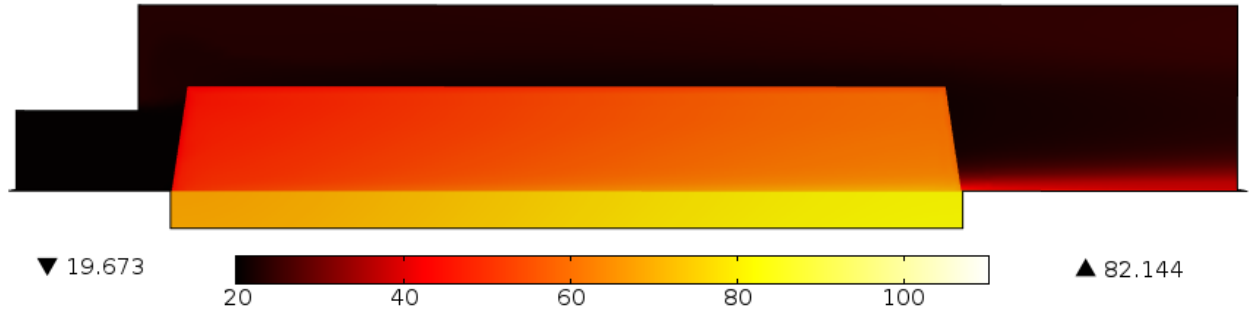

4) Fin height 52mm

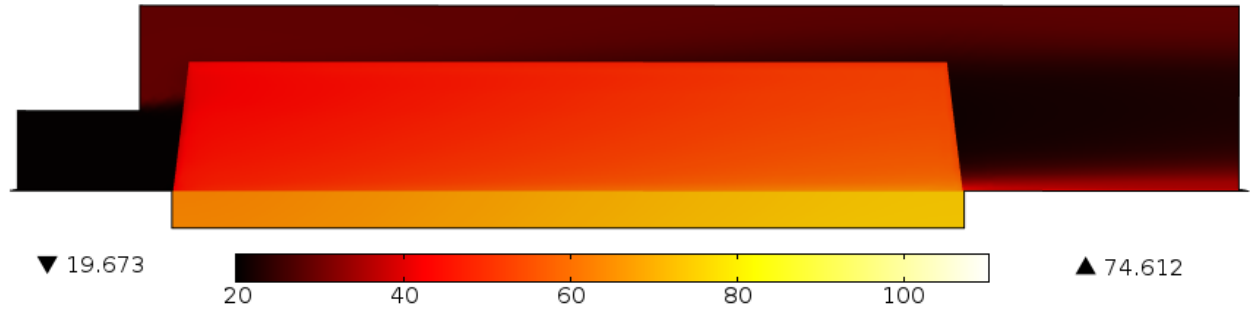

5) Fin thickness 1mm

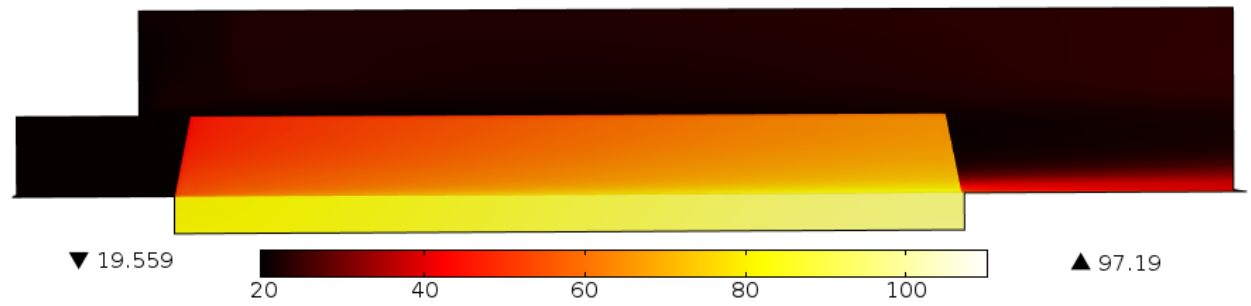

5) Fin thickness 5mm

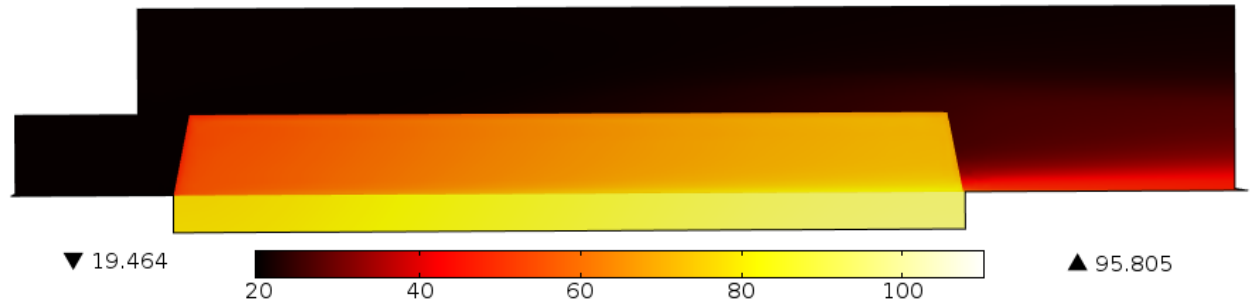

7)

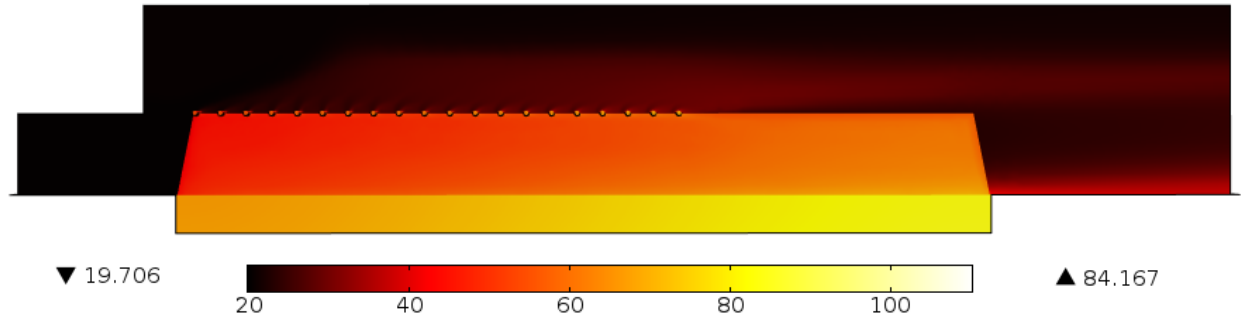

8)

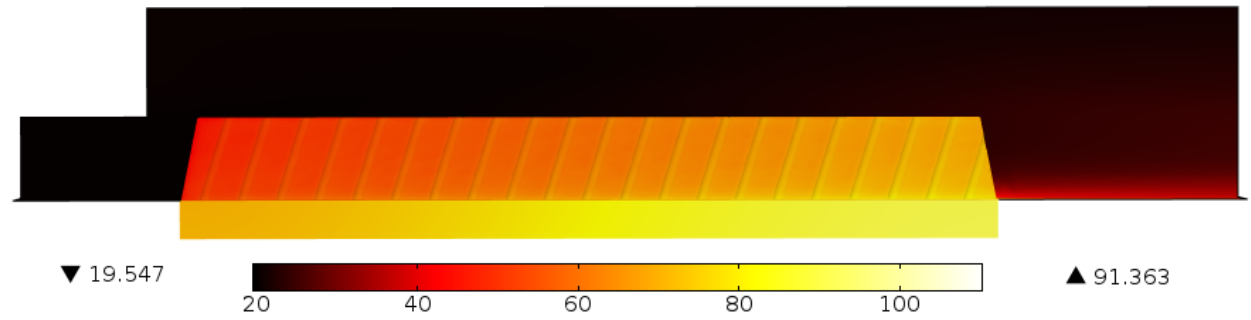

9)

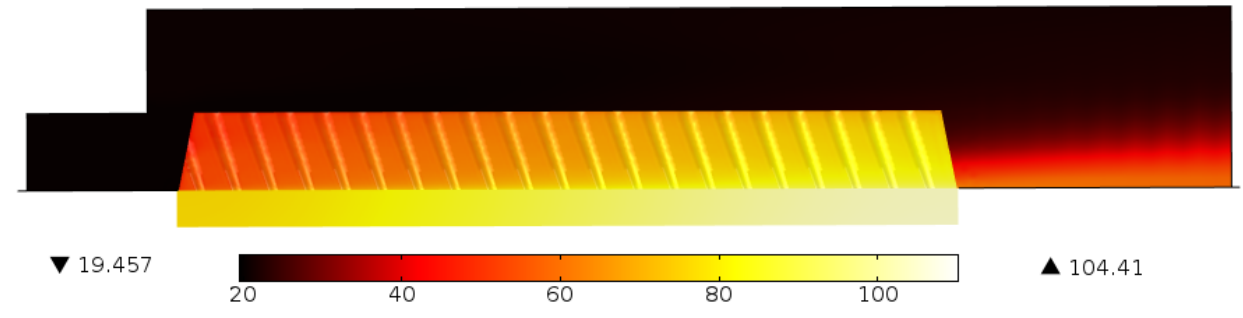

10)

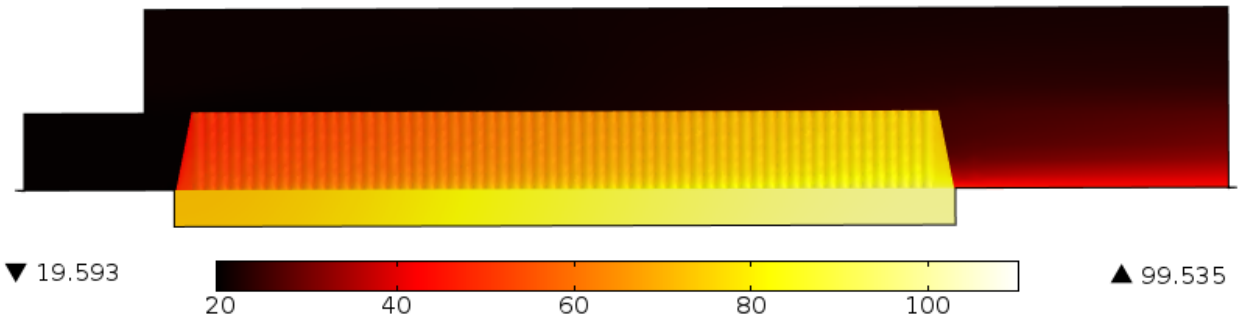
▼ 19.593
20
40
60
80
100
▲ 99.535

11)

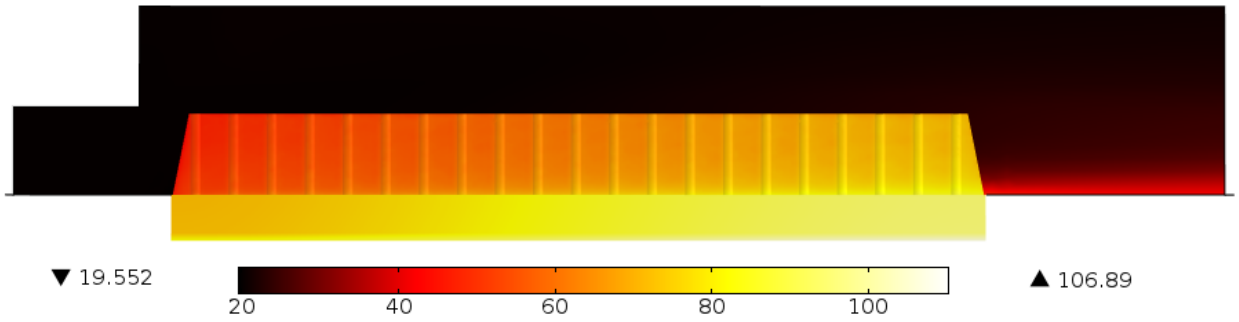
▼ 19.552
20
40
60
80
100
▲ 106.89

12)

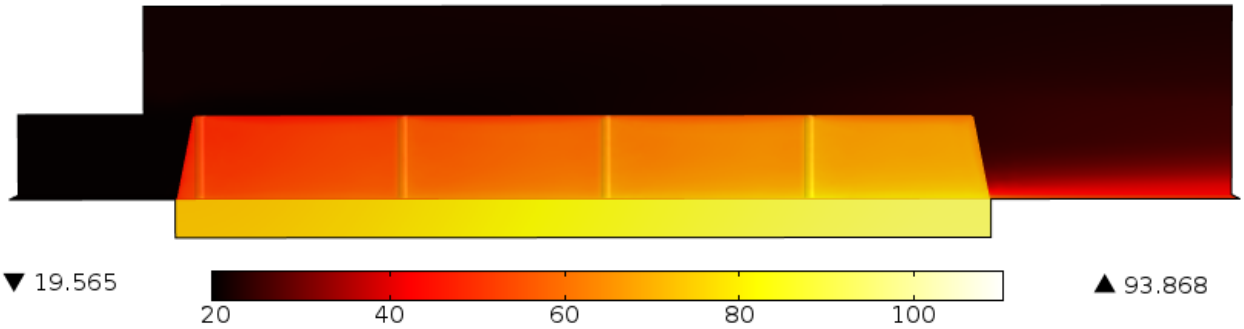
▼ 19.565
20
40
60
80
100
▲ 93.868

13)

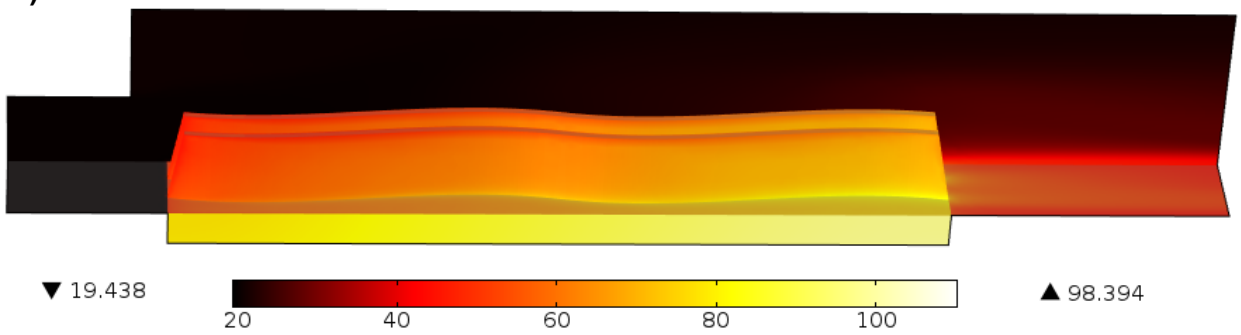
▼ 19.438
20
40
60
80
100
▲ 98.394

14)

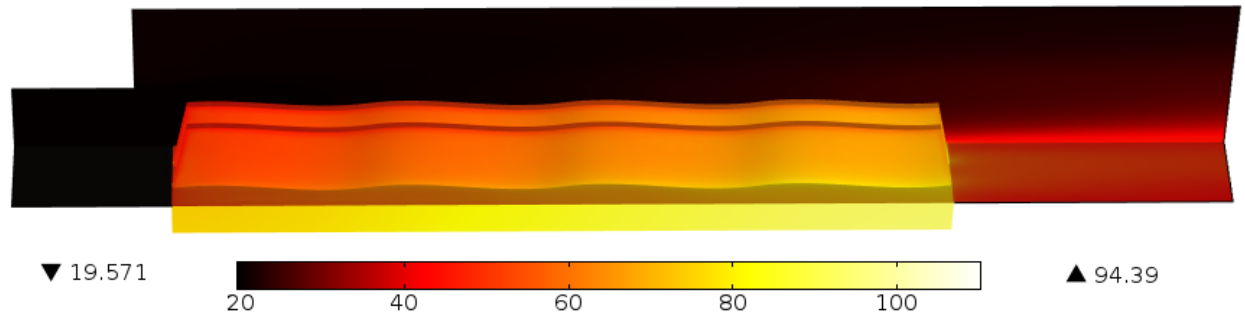
▼ 19.571
20
40
60
80
100
▲ 94.39

15)

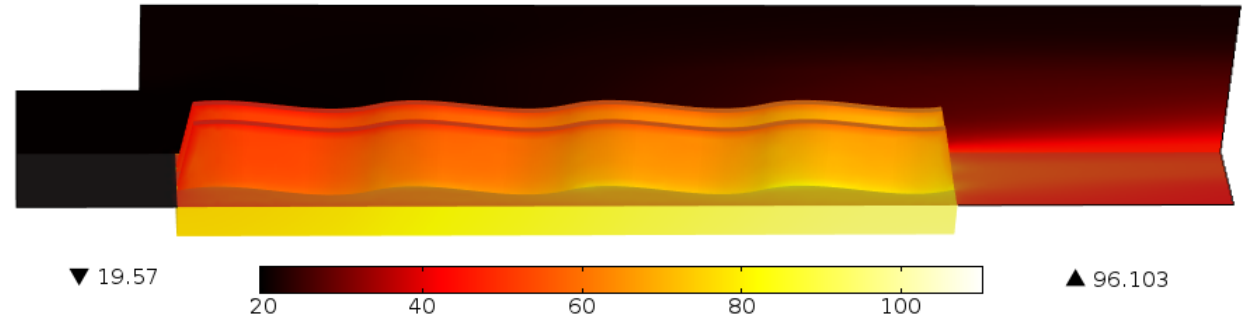
▼ 19.57
20
40
60
80
100
▲ 96.103

16)

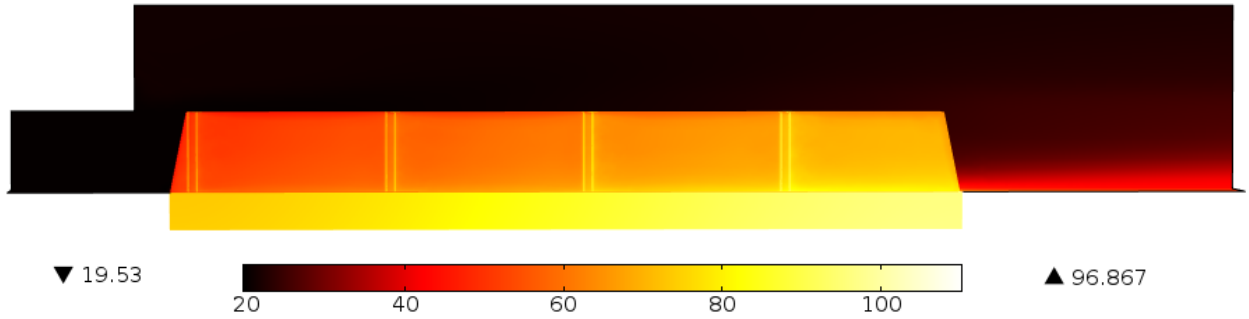
▼ 19.53
20
40
60
80
100
▲ 96.867

Appendix 5

testo

Kalibrier-Protokoll
Certificate of conformity • Protocole d'étalonnage
Protocollo di collaudo • Informe de calibración

Gerät / Module type / Type de modèle / Modelo: **testo 950/650/400**

Serien-Nummer / Serial No. / No. de série / Número de serie: **01299222**

Schnittstellentest / Interface test / Test d'interface / Test interface:	ok
Druckertest / Printercheck / Test de l'imprimeur / Test de impresora:	ok
Segmenttest / Display test / Test d'affichage / Test del visualizador:	ok
Akkuladung / Recharching battery / Charge d'accus / Batería recargable:	ok
Stromaufnahme / Power supply / Alimentation / Alimentación:	ok
Kanal1/2 / Channel1/2 / Canal1/2 / Canal1/2:	ok

Meßwerte ohne Meßfühler / Measured values without probe /
Valeurs mesurées sans sonde de mesure / Valores medidos sin sonda de medición:

Sollwert Reference Référence Referencia	Zulässige Toleranz Permissible tolerance Tolérance admise Tolerancia permitida	Istwert Actual Value Valeur réelle Valor medido
Typ K / Type K / Type K / Tipo K		
-100.0 °C	± 0.4 °C	-100.0 °C
0.0 °C	± 0.4 °C	0.0 °C
200.0 °C	± 0.4 °C	200.0 °C
900.0 °C	± 1.0 °C	900.0 °C
NTC / NTC / CNT / NTC		
50.0 °C	± 0.2 °C	50.0 °C
Pt100 / Pt100 / Pt100 / Pt100		
80.0 °C	± 0.1 °C	79.9 °C
thermisch / hotwire / file chaude / hilo caliente		
10.00 m/s	± 0.04 m/s	10.00 m/s
Druck 100hPa / pressure 100hPa / Pression 100hPa / Presión 100hPa		
80.00 hPa	± 0.10 hPa	80.00 hPa
relative Luftfeuchte / relative humidity / humidité relative / humedad relativa		
12.0 %	± 1 Digit	12.0 %

Datum/Date/Data/Fecha: 27.11.06 **Prüfer/Inspector/Vérificateur/Verificatore/Verificador: 642**

Genauigkeit Hitzkugelsonden

Accuracy hot bulb probes
Précision sondes à boules chaudes

Hitzkugelsonden, abgeglichen im Freistrahl Ø 350 mm
Hot bulb probes, adjusted in a free jet diam. 350 mm
Sondes à boules chaudes, ajustées en jet libre diàm. 350 mm

Bezugsdruck 1013 hPa, Bezugstemperatur 22 °C
Reference pressure 1013 hPa, reference temperature 22 °C
Pression de référence 1013 hPa, température de référence 22 °C

bezogen auf testo Referenz DKD-Labor-Strömung
referring to the testo reference DKD laboratory for velocity
Anémomètre de référence labo DKD pour les mesures de vitesse d´air

Best.-Nr. *Order no.* *Réf.*	*Meßbereich* *Measuring range* *Etendue de mesure*	*Genauigkeit* *Accuracy* *Précision*
0635.1549	m/s: 0...10,00 m/s °C: -20,0...70,0 °C	± (0,03 m/s + 5% v. Mw./of mv/v.m.) (0...10,00 m/s)
0635.1049	m/s: 0...10,00 m/s C: -20,0...70,0 °C	
0635.1045 für/for/pour **testo 452**	m/s: 0...10,00 m/s °C: -20,0...70,0 °C %rF: 0...100 % nicht betauen! not to be dewed! ne pas roser!	Temperaturkompensation besser als Temperature compensation better than Température de compensation mieux que ± 0,2 % v. Mw./°C / of mv/°C / v.m./°C (-10...60 °C)
0635.1540 für/for/pour **testo 400**		
0628.0035	m/s: 0...10,00 m/s C: -20,0...70,0 °C	

0973.0403/02.02/T/wh/09.02.2004

Testo gleicht die thermischen Sonden auf einen Referenzdruck von 1013 hPa ab. Weicht in der praktischen Anwendung der Umgebungs- bzw. Prozeßdruck vom Referenzdruck (1013 hPa) ab, kann beim **testo 400** der Absolutdruck zur automatischen Druckkompensation direkt eingegeben werden. Bei anderen Geräten ergibt sich die wahre Geschwindigkeit aus der Formel:

$$V_{wahr} = V_{Anzeige} * \text{Korrekturfaktor} \quad \text{bzw.}$$

$$V_{wahr} = V_{Anzeige} * \frac{1013\ [hPa]}{\text{Umgebungsdruck [hPa]}}$$

The thermal sensors are calibrated by Testo with a reference pressure of 1013 hPa.
If the ambient or process pressure applied in practice deviates from the reference pressure (1013 hPa), the absorption pressure in the case of **testo 400** can be input directly for automatic pressure compensation. The real velocity in other instruments can be calculated from the following formula:

$$V_{real} = V_{indicated} * \text{Correction factor} \quad \text{or}$$

$$V_{real} = V_{indicated} * \frac{1013\ [hPa]}{\text{Ambient pressure [hPa]}}$$

Les capteurs thermiques sont étalonnés avec une pression de réference du 1013 hPa.
Si la pression ambiante ou la pression de processus se différencient de la pression de réference (1013 hPa), la compensation automatique de la pression absolue peut être modifiée directement sur le **testo 400**. Pour d´autres appareils, la vitesse réelle est déterminée par la formule suivante.

$$V_{vraie} = V_{indiquée} * \text{Coefficient de correction} \quad \text{ou}$$

$$V_{vraie} = V_{indiquée} * \frac{1013\ [hPa]}{\text{La pression ambiante (hPa)}}$$

Ortshöhe (m)	mittlerer Luftdruck (hPa)	Korrektur-faktor
Location height	**Average air pressure**	**Correction factor**
L´hauteur de la position	**Pression d´air moyenne**	**Coefficient de correction**
500	954	1,061
600	943	1,074
700	932	1,087
800	921	1,100
900	909	1,114
1000	898	1,127
1100	888	1,141
1150	882	1,148
1200	877	1,155
1250	872	1,162
1300	866	1,169
1350	861	1,177
1400	856	1,184
1450	850	1,191
1500	845	1,198
1550	840	1,206
1600	835	1,213
1650	830	1,221
1700	825	1,228
1750	820	1,236
1800	815	1,244
1850	810	1,251
1900	805	1,259
1950	800	1,257
2000	795	1,275
2050	790	1,283
2100	785	1,291
2150	780	1,299
2200	775	1,307
2250	770	1,315
2300	766	1,323
2350	761	1,332
2400	756	1,340
2450	751	1,348
2500	747	1,357
2550	742	1,365